Please cite this article in press as: Wade et al., Mutations in *MAP3K7* that Alter the Activity of the TAK1 Signaling Complex Cause Frontometaphyseal Dysplasia, The American Journal of Human Genetics (2016), http://dx.doi.org/10.1016/j.ajhg.2016.05.024

ARTICLE

Mutations in *MAP3K7* that Alter the Activity of the TAK1 Signaling Complex Cause Frontometaphyseal Dysplasia

Emma M. Wade,[1] Philip B. Daniel,[1] Zandra A. Jenkins,[1] Aideen McInerney-Leo,[2] Paul Leo,[2] Tim Morgan,[1] Marie Claude Addor,[3] Lesley C. Adès,[4] Debora Bertola,[5] Axel Bohring,[6] Erin Carter,[7] Tae-Joon Cho,[8] Hans-Christoph Duba,[9] Elaine Fletcher,[10] Chong A. Kim,[5] Deborah Krakow,[11] Eva Morava,[12] Teresa Neuhann,[13] Andrea Superti-Furga,[14] Irma Veenstra-Knol,[15] Dagmar Wieczorek,[16] Louise C. Wilson,[17] Raoul C.M. Hennekam,[18] Andrew J. Sutherland-Smith,[19] Tim M. Strom,[20] Andrew O.M. Wilkie,[21] Matthew A. Brown,[2] Emma L. Duncan,[2] David M. Markie,[22] and Stephen P. Robertson[1,*]

Frontometaphyseal dysplasia (FMD) is a progressive sclerosing skeletal dysplasia affecting the long bones and skull. The cause of FMD in some individuals is gain-of-function mutations in *FLNA,* although how these mutations result in a hyperostotic phenotype remains unknown. Approximately one half of individuals with FMD have no identified mutation in *FLNA* and are phenotypically very similar to individuals with *FLNA* mutations, except for an increased tendency to form keloid scars. Using whole-exome sequencing and targeted Sanger sequencing in 19 FMD-affected individuals with no identifiable *FLNA* mutation, we identified mutations in two genes—*MAP3K7,* encoding transforming growth factor β (TGF-β)-activated kinase (TAK1), and *TAB2,* encoding TAK1-associated binding protein 2 (TAB2). Four mutations were found in *MAP3K7*, including one highly recurrent (n = 15) de novo mutation (c.1454C>T [p.Pro485Leu]) proximal to the coiled-coil domain of TAK1 and three missense mutations affecting the kinase domain (c.208G>C [p.Glu70Gln], c.299T>A [p.Val100Glu], and c.502G>C [p.Gly168Arg]). Notably, the subjects with the latter three mutations had a milder FMD phenotype. An additional de novo mutation was found in *TAB2* (c.1705G>A, p.Glu569Lys). The recurrent mutation does not destabilize TAK1, or impair its ability to homodimerize or bind TAB2, but it does increase TAK1 autophosphorylation and alter the activity of more than one signaling pathway regulated by the TAK1 kinase complex. These findings show that dysregulation of the TAK1 complex produces a close phenocopy of FMD caused by *FLNA* mutations. Furthermore, they suggest that the pathogenesis of some of the filaminopathies caused by *FLNA* mutations might be mediated by misregulation of signaling coordinated through the TAK1 signaling complex.

Introduction

Frontometaphyseal dysplasia (FMD [MIM: 305620]) is a progressive sclerosing skeletal dysplasia characterized by supraorbital hyperostosis, undermodeling of the long bones, small and large joint contractures, and other extraskeletal developmental abnormalities, most notably of the cardiorespiratory system and genitourinary tract.[1] An X-linked form of FMD has been clearly defined, and in this condition, males manifest most prominently, although females can express a milder phenotype that includes hyperostosis and limb anomalies.[2,3] The severity of the disorder in males can extend from normal stature with near-normal adaptive functioning to perinatal lethality, principally due to the consequences of the extraskeletal malformations.[3] The hyperostosis observed in FMD is not associated with bone fragility, and the excess cortical bone has the histological appearance of mature lamellar bone.

Gain-of-function mutations in *FLNA* (MIM: 300017), located on the X chromosome and encoding the actin-binding protein filamin A, account for FMD in ~50% of individuals.[3] This form of the condition is allelic to a spectrum of related phenotypes known as the otopalatodigital spectrum disorders (OPDSDs).[2,4] The mutations leading to OPDSDs are principally missense and small in-frame

[1]Department of Women's and Children's Health, Dunedin School of Medicine, University of Otago, Dunedin 9016, New Zealand; [2]Royal Brisbane and Women's Hospital, Herston, QLD 4029, Australia; [3]Service de Génétique Médicale Maternité, CHUV, Lausanne 1011, Switzerland; [4]Discipline of Pediatrics and Child Health and Department of Clinical Genetics, University of Sydney and The Children's Hospital, Westmead, Sydney, NSW 2145, Australia; [5]Genetics Unit, Instituto da Criança, Hospital das Clinicas da Faculdade de Medicina, São Paulo 05403-000, Brazil; [6]Institut fur Humangenetik, Universitatsklinikum Munster, Munster 48149, Germany; [7]Kathryn O. and Alan C. Greenberg Center for Skeletal Dysplasias, Hospital for Special Surgery, New York, NY 10021, USA; [8]Division of Pediatric Orthopedics, Seoul National University Children's Hospital, Seoul 28, Republic of Korea; [9]Zentrum Medizinische Genetik Linz, Med Campus IV, Kepler Universitätsklinikum, Krankenhausstrasse, 26–30, 4020 Linz, Austria; [10]South East Scotland Clinical Genetics Service, Western General Hospital, Edinburgh EH4 2XU, UK; [11]David Geffen School of Medicine, UCLA, Los Angeles, CA 90095, USA; [12]Hayward Genetics Center, Tulane University Medical School, New Orleans, LA 70112 USA; [13]MGZ–Medical Genetics Center, Munich 80335, Germany; [14]Department of Pediatrics, CHUV and University of Lausanne, Lausanne 1015, Switzerland; [15]University Medical Center, Groningen 9713, the Netherlands; [16]Institute of Human Genetics, Heinrich Heine University, Dusseldorf 40225, Germany; [17]Clinical Genetics Unit, Great Ormond Street Hospital for Children NHS Foundation Trust, London WC1N 3JH, UK; [18]Department of Pediatrics, Academic Medical Center, University of Amsterdam, Amsterdam 1105, Netherlands; [19]Institute of Fundamental Sciences, Massey University, Palmerston North 4474, New Zealand; [20]Institut für Humangenetik, Helmholtz Zentrum München, Neuherberg, Munich 85764, Germany; [21]Weatherall Institute of Molecular Medicine, University of Oxford and John Radcliffe Hospital, Headington, Oxford OX3 9DS, UK; [22]Department of Pathology, Dunedin School of Medicine, University of Otago, Dunedin 9016, New Zealand
*Correspondence: stephen.robertson@otago.ac.nz
http://dx.doi.org/10.1016/j.ajhg.2016.05.024.

Please cite this article in press as: Wade et al., Mutations in *MAP3K7* that Alter the Activity of the TAK1 Signaling Complex Cause Frontometaphyseal Dysplasia, The American Journal of Human Genetics (2016), http://dx.doi.org/10.1016/j.ajhg.2016.05.024

deletions and insertions that are clustered throughout the coding regions of *FLNA*, some of which are highly recurrent.[2,5,6] Many of these mutations, including some leading to FMD,[3] result in the substitution of residues in the N-terminal actin-binding domain of the protein. The effect of FMD-associated mutations on the function of this domain has not been explicitly addressed, but a recurrent missense mutation leading to the allelic disorder otopalatodigital syndrome type 2 (OPD2 [MIM: 304120]) confers enhanced avidity for actin.[7] How this activity results in malformations in addition to hyperostosis is unknown, but the mechanism could relate to one or more of the many and varied biochemical functions of filamin A that include engagement with integrin-mediated cell-cell adhesion,[8–10] cytoskeletal remodeling,[11,12] cell spreading and migration,[13] mechanotransduction,[14,15] and influencing many cell signaling pathways through physical interactions with a multiplicity of second messenger proteins.[16]

Around 50% of individuals with a diagnosis of FMD have no demonstrable mutation in *FLNA*.[3,17] These individuals are almost indistinguishable phenotypically from those with *FLNA*-mutation-positive FMD,[3,17] one notable difference being the preponderance for individuals without an identifiable *FLNA* mutation to develop keloid scarring. Unlike X-linked FMD, the severity of the phenotype does not vary between the sexes, although females are more likely to develop keloid, similar to the presentation of this sporadically arising cutaneous condition.[17] The majority of individuals with the FMD phenotype not explained by a *FLNA* mutation are isolated cases in their families; only rare instances of vertical transmission of the phenotype have been reported.[3,17,18]

Here, we analyze 19 individuals with FMD who do not have an identifiable *FLNA* mutation and find mutations in two genes encoding components of the transforming growth factor β (TGF-β)-activated kinase (TAK1) signaling complex in all subjects. Strikingly, 15 individuals have a recurrent mutation in *MAP3K7* (MIM: 602614), which encodes for TAK1. We show that these mutations result in enhanced TAK1 autophosphorylation and alteration of MAPK and NF-κB signal transduction emanating from this protein complex. Three additional individuals have missense mutations in the *MAP3K7* region that encodes the kinase domain. These mutations produce a notably milder phenotype, which suggests a domain-specific phenotype-genotype correlation in this form of FMD. These results place TAK1 as a key regulator of several cell signaling pathways that coordinately regulate osteogenesis.

Material and Methods

Subject Ascertainment and Ethical Approval

Individuals with FMD were recruited by physician-initiated referral and consented to participate under approved protocols MEC/08/08/094 and 13/STH/56 (Health and Disability Ethics Committee, New Zealand). Subjects were diagnosed with FMD on the basis of clinical and radiological assessment, according to published criteria.[3] Sanger sequencing of *FLNA* did not detect any mutations. Where possible, DNA was also collected from parents and siblings, and familial relationships were confirmed as declared by the examination of the segregation of six unlinked microsatellite markers.

Whole-Exome Sequencing

Identification of candidate genetic variants was initially performed with exome sequence data from parent-proband trios for four simplex individuals (01, 02, 05, and 17). Additional Sanger and exome sequencing was carried out on samples from the remaining 15 subjects. Genomic DNA was extracted from peripheral blood according to standard protocols. Parental DNA was available from ten families.

For three trios (subjects 01, 02, and 05 and their parents), exome enrichment was performed with the Agilent SureSelect Human All Exon V4+UTRs capture kit, and paired-end sequencing (generating 100 base-pair reads) was performed on the Illumina HiSeq2000 sequencing platform. Sequencing data were aligned to the Ensembl Genome browser human genome assembly (GRCh37) with the Burrows-Wheeler Aligner (MEM algorithm) v.0.7.12. Realignment around indels, marking of duplicate reads, and recalibration of base quality scores, was undertaken with tools from Picard v.1.140 (Broad Institute) and the Genome Analysis Toolkit (GATK) v.3.4-46 (Broad Institute). Individual variant calling was undertaken with the GATK HaplotypeCaller and followed by multisample genotyping and variant quality score recalibration. Gene context annotation was added with SnpEff v.4.1L, and allele frequencies were obtained from 1000 Genomes Project phase 1, NHLBI GO Exome Sequencing Project ESP6500, and the Exome Aggregation Consortium (ExAC) via the GATK VariantAnnotator. Sequential filtering of the multisample VCF file was undertaken with GATK SelectVariants and SnpSift v.4.1L (SnpEff). Subsequently, this protocol was carried out on individual 14. For samples from subjects 17, 18, and 19 and their respective parents, exome enrichment was performed with an Illumina TruSeq Exome Enrichment kit. Massively parallel sequencing was performed with the Illumina HiSeq2000 platform, generating 100 base-pair paired-end reads. Demultiplexing, base calling, alignment, variant calling, and annotation of these trios was performed as described previously.[19] For all individuals analyzed by exome sequencing, platform artifacts were removed and good quality, rare variants (minor allele frequency < 0.001) in coding regions (including splice sites and 5′ and 3′UTRs) were retained (Table S4). De novo variants (present in the affected child but not in either parent) were then identified for each individual. Candidate mutations, and their de novo status, were confirmed by Sanger sequencing in subjects and their parents. Samples from subject 12 and their parents were exome sequenced with a slightly different protocol and analytical pipeline that has been described previously.[20] Directed Sanger sequencing of the two candidate genes was performed in 12 additional individuals (for primer sequences, see Table S1).

cDNA Preparation and RT-PCR

Primary dermal fibroblasts from individuals with *MAP3K7*-mutation-positive FMD were cultured in DMEM (Gibco, Thermo Fisher), plus 10% fetal bovine serum (FBS; Moregate) and 1% streptomycin and penicillin (Gibco). RNA was extracted with Trizol reagent (Thermo Fisher) and the Nucleospin RNA kit (Machery-Nagel), according to kit protocols. cDNA was reverse-transcribed from total RNA with the SuperScriptIII kit (Thermo

Fisher), according to the kit protocol. PCR amplification and Sanger sequencing was carried out with primers listed in Table S1.

Generation of Expression Constructs

The full coding sequence of *MAP3K7* (variant A[21] [GenBank: NM_003188.3]) was amplified from HEK293 cDNA with primer pair 1 (for all primer sequences, see Table S2) and cloned into pcDNA3.1 with the TOPO cloning kit (Thermo Fisher). This transcript was selected for these studies because (1) it represents the form that contains exon encoding sequences subject to mutation in the disorder under study, and (2) it represents the isoform studied by the vast majority of investigations into the properties of this gene. Primer pairs two, three, and four were used to sub-clone *MAP3K7* into EcoRI- and XbaI-restriction-digested pCMV-Myc, pCMV-HA, and p3xFLAG-CMV with the Gibson assembly kit (NE Biolabs). *TAB2* (GenBank: NM_015093.5) was amplified from HEK293 cDNA with primer pair four and cloned into pcDNA3.1 with TOPO cloning. Primer pair 5 was utilized for the sub-cloning of *TAB2* into EcoRI- and XbaI-digested pCMV-HA with the Gibson assembly. *TAB1* (pT7-FLAG) was a kind gift from K. Matsumoto (Nagoya University). Mutagenesis in *MAP3K7* was carried out with overlapping amplicons containing the mutagenized base, followed by Gibson Assembly.

Co-immunoprecipitation

For competitive co-immunoprecipitation of TAK1 and TAB2, HEK293FT cells were cultured in DMEM (Gibco) plus 10% FBS (Moregate) and co-transfected with one of the following, using Lipofectamine2000 (Thermo Fisher) in a 24-well plate: (1) pCMV-HA TAB2 (800 ng), pCMV-MYC TAK1 (10 ng), and p3XFLAG TAK1 (10 ng), (2) pCMV-HA TAB2 (800 ng), pCMV-MYC TAK1 (10 ng), and p3XFLAG TAK1 p.Pro485Leu (10 ng), (3) pCMV-MYC TAK1 (10 ng) and p3XFLAG TAK1 (10 ng), or (4) pCMV-MYC TAK1 (10 ng) and p3XFLAG TAK1 p.Pro485Leu (10 ng). For analysis of TAK1 dimerization by competitive co-immunoprecipitation, HEK293FT cells were co-transfected with one of the following, using the same protocol: (1) pCMV-HA TAK1 (250 ng), pCMV-MYC TAK1 (250 ng), and p3XFLAG TAK1 (250 ng) or (2) pCMV-HA TAK1 (250 ng), pCMV-MYC TAK1 (250 ng), and p3XFLAG TAK1 p.Pro485Leu (250 ng). After 20 hr, cells were lysed in 1× PBS and 1% Triton X^{100} with protease inhibitor (cOmplete mini, Roche). Lysates were clarified by centrifugation and 30 μL was retained for input samples. 2 μL of mouse anti-HA (Sigma Aldrich, H3663) was added to 150 μL supernatant, and samples were mixed at 4°C for 4 hr. 50 μl of washed Protein G Dynabeads (Thermo Fisher) were added to each sample and incubated for a further 30 min at 4°C, followed by three 1 mL washes in PBS. Protein was eluted in SDS sample buffer, and samples were resolved by 7% SDS-PAGE, followed by transfer to a nitrocellulose membrane. Membranes were blocked in 5% milk (PBS) then incubated with either mouse anti-HA (1:5,000, Sigma Aldrich, H3663), mouse anti-MYC (1:5,000, Clontech, 631206), or mouse anti-FLAG (1:7,000, Sigma Aldrich, F1804), followed by secondary goat anti-mouse IRDye 800CW (1:25,000, LI-COR, 926-32210). Membranes were scanned on a LI-COR Odyssey Clx, and bands were quantified with LI-COR Image Studio Lite software.

Luciferase Assays

HEK293 cells were cultured as previously described and transfected in a 24-well plate with 100 ng of plasmid DNA per well with Lipofectamine2000. Transfections were harvested 20 hr later in passive lysis buffer and assayed for Renilla and firefly luciferase activities with a Synergy2 multi-mode reader (BioTek) and injector module, which delivered the respective luciferase assay buffers (Promega). MAPK activity was assayed with the pFR-luc and pFA-ELK1 Pathdetect vectors (Agilent), which detect MAPK phosphorylation of the GAL4-ELK1 fusion protein and subsequent transcription from the pFR-luc reporter. NF-kB activity was measured from the reporter pNF-κBREluc (pGL4.32 [luc2P/NF-kB-RE/Hygro]; Promega). DNA constructs were transfected with the following amounts (ng/well): pFRluc (10), pFA-ELK1 (10), pNF-κBREluc (5), pSVminRL (10–45), pTAK1 and mutants (10), pHA-TAB2 and mutant (40), and pCR3.1 (as empty vector) (10–50).

Western Blotting

For TAK1 stability, HEK293FT cells were transfected with 20 ng p3XFLAG TAK1 (wild-type [WT], p.Pro485Leu, or p.Gly168Arg) and treated with 85 μg/mL cycloheximide in DMSO or equivalent DMSO control after 24 hr. For quantification of phospho-TAK1, HEK293FT cells were transfected with 40 ng pCMV-HA TAB2 (WT or p.Glu569Lys), 20 ng pT7-FLAG TAB1, and 20 ng p3XFLAG TAK1 (WT and mutants) with Lipofectamine2000 in a 24-well plate. Transfections for phosphorylated p38 (p-p38) western blots were carried out as for luciferase assays. After 24 hr, cells were lysed in 1× PBS and 1% Triton X^{100} with protease inhibitor; supernatant was cleared by centrifugation. Samples were denatured in 2.3% SDS and 1% DTT buffer. Proteins were resolved by electrophoresis on 8% polyacrylamide gels, followed by transfer to nitrocellulose membrane. Membranes were blocked in 5% milk (PBS) or Odyssey PBS buffer (LI-COR) and probed for 1 hr to overnight with anti-FLAG (F1804, Sigma Aldrich; 1:7000), anti-Myc (631206, Takara/Clontech; 1:5000), anti-phospho-TAK1 (Thr187, 1:1,500, Cell Signaling, CST4536), anti-p38 (1:2,000, Cell Signaling, CST9212), or anti-p-p38 (Thr180/Tyr182, CST9216, Cell Signaling Technologies; 1:4000). Detection was done with secondary goat anti-mouse IRDye 800CW (1:25,000, LI-COR, 926-32210) and goat anti-rabbit IRDye 700CW (1:25,000, LI-COR, 926-68071) antibodies as described above.

Statistical Analysis

Quantitative data from western blots and luciferase assays was imported into Excel and scaled and normalized to appropriate controls. Two-way, unpaired t tests were carried out, and critical p values were Bonferroni corrected (*$p \leq 0.05$, **$p \leq 0.01$, ***$p \leq 0.001$).

Results

Individuals with FMD with and without *FLNA* Mutations are Phenotypically Similar

We ascertained a cohort of 19 individuals with FMD without *FLNA* mutations. Clinically, they are very similar to FMD individuals with *FLNA* mutations, apart from an increased incidence of keloid formation[17,18] (Figure 1, Table 1). Core features of the phenotype include prominent supraorbital ridges, hyperostosis, downslanting palpebral fissures, hypertelorism, and a wide nasal bridge. The chin is typically small and pointed (Figure 1A). Progressive contractures of the joints are

Please cite this article in press as: Wade et al., Mutations in *MAP3K7* that Alter the Activity of the TAK1 Signaling Complex Cause Frontometaphyseal Dysplasia, The American Journal of Human Genetics (2016), http://dx.doi.org/10.1016/j.ajhg.2016.05.024

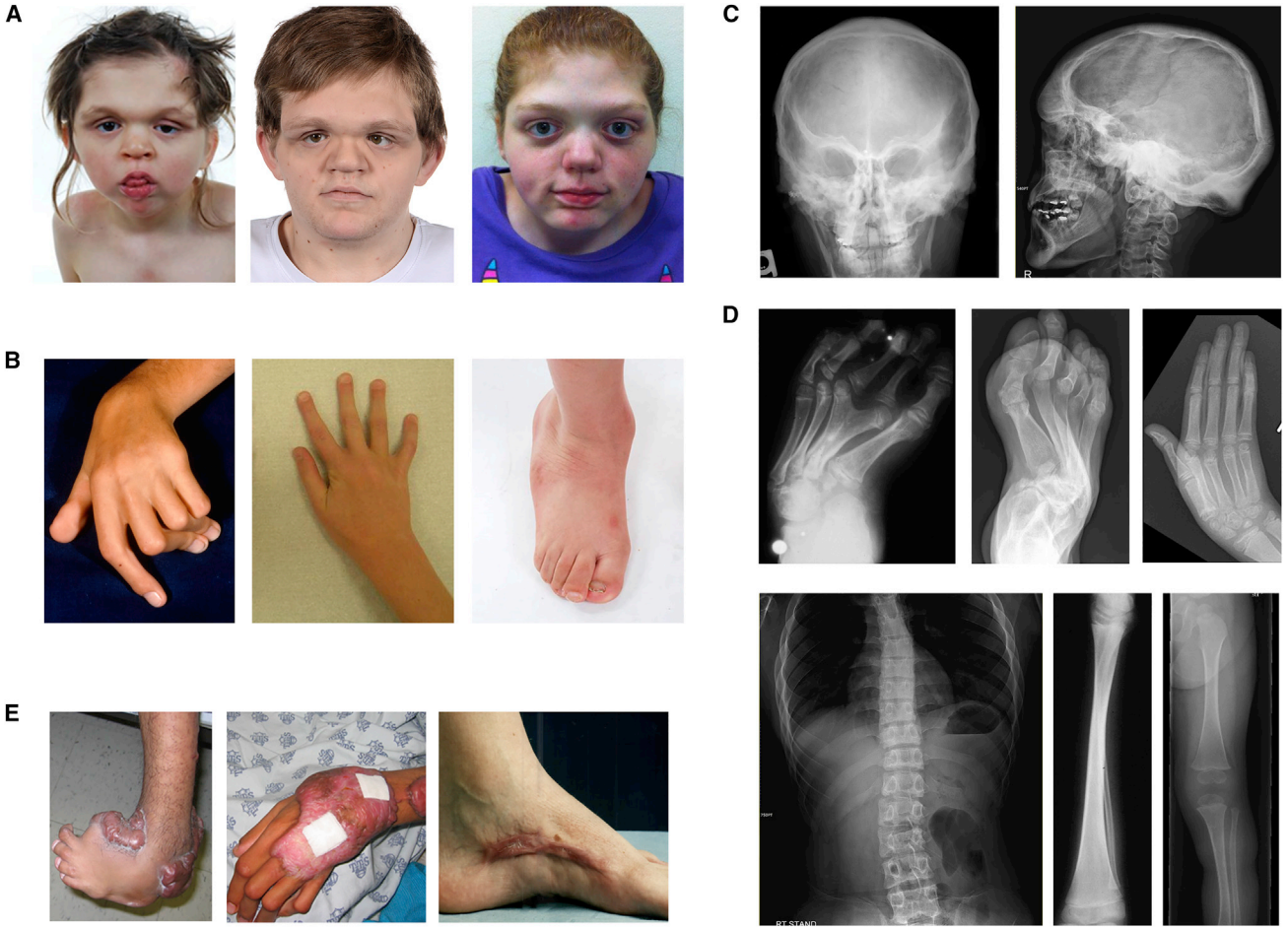

Figure 1. Clinical Images of Individuals with FMD
(A) Characteristic facial features, including supraorbital hyperostosis, downslanting palpebral fissures, hypertelorism, a broad nasal bridge, and a small pointed chin. Panels, from left to right, show subjects 14, 05, (both TAK1 p.Pro485Leu), and 17 (TAB2 p.Glu569Lys).
(B) Limb abnormalities include contractures of the metacarpophalangeal and interphalangeal joints (subjects 01 and 17) and valgus deformity of the foot (subject 14).
(C and D) Radiological assessment reveals (C) a dense, sclerotic skull, especially around the frontal bone and skull base (subjects 09 and 08) and (D) undermodeled phalanges, metatarsals, and metacarpals (subjects 01, 05, and 13) with occasional metacarpal synostosis (subject 01), scoliosis and undermodeled ribs (subject 08), and splaying of the metaphysis of the tibia and femur with bowing (subjects 01 and 02).
(E) Keloid scar formation in subjects 11 and 05.

common, especially in the fingers and wrists (Figure 1B). Radiographs show a dense skull, especially the frontal bone and skull base (Figure 1C). The long bones of the hands and feet are undermodeled, frequently with sclerotic cortices (Figure 1D). Subjects often present with mild to severe scoliosis and have undermodeled, deformed ribs, sometimes with a "coat-hanger" configuration. The long bones have dense cortices and splaying of the metaphyses (Figure 1D). Three subjects had a somewhat milder skeletal phenotype (07, 18, and 19; Table 1), and individual 07 lacked a number of facial characteristics but still had prominent supraorbital ridges. Of the 19 individuals listed in Table 1, eight (two male, six female) exhibit keloid scarring that is occasionally progressive and severe and has the potential to form either spontaneously or after surgical trauma (Figure 1E).

Mutations in *MAP3K7* and *TAB2* Cause FMD

Whole-exome sequencing in family trios identified three individuals (01, 02, and 05) with the same de novo missense mutation, c.1454C>T, in *MAP3K7* ([GenBank: NM_003188.3] Table 2). The subjects each had no more than three non-synonymous, validated de novo mutations in total across their respective exomes (Tables S3–S4). The recurrent mutation is predicted to substitute a proline to a leucine at position 485 (p.Pro485Leu) of the protein product of *MAP3K7*, TAK1. Subsequently, an additional individual (subject 12) was independently found, via exome analysis, to have the same de novo mutation.

Sequencing of another family trio (subject 17, Figure 1A, right panel) demonstrated a de novo missense variant, c.1705G>A, in *TAB2* (MIM: 605101 [GenBank: NM_015093.5]), which encodes the binding partner of TAK1, TAK1-associated binding protein 2 (TAB2).[22] This

Please cite this article in press as: Wade et al., Mutations in *MAP3K7* that Alter the Activity of the TAK1 Signaling Complex Cause Frontometaphyseal Dysplasia, The American Journal of Human Genetics (2016), http://dx.doi.org/10.1016/j.ajhg.2016.05.024

variant substitutes a glutamic acid to a lysine at position 569 (p.Glu569Lys) of TAB2 and was confirmed by Sanger sequencing. This individual had one other de novo variant in *EFHC1*: c.674C>G (p.Thr225Ser [GenBank: NM_018100.3]). Missense mutations in this region of *EFHC1* are associated with juvenile absence or myoclonic epilepsy.[23,24] Because individual 17 has no history of seizures and because *TAB2* is known to directly interact with and stabilize TAK1,[22] the *TAB2* mutation was prioritized for further analysis.

Further exome analysis and targeted Sanger sequencing of the exons of *MAP3K7* and *TAB2* in the remaining individuals with unsolved cases of FMD found that another 11 individuals have the recurrent c.1454C>T *MAP3K7* mutation and an additional subject (07) was found to have novel de novo mutation in *MAP3K7*: c.502G>C, predicting the substitution p.Gly168Arg in TAK1 (Table 2). In addition, two unrelated individuals (18 and 19) who share the FMD phenotype with their respective mothers were found to have missense mutations in *MAP3K7*: c.208G>A and c.299T>A, predicting the substitutions p.Glu70Gln and p.Val100Glu, respectively. Both of these mutations were shown to have been inherited from the proband's affected mother. In both instances, maternal grandparental samples were not available to ascertain if they had arisen de novo or not.

The phenotype of individuals with the recurrent c.1454C>T mutation is not noticeably different from that of subject 17, who has the missense mutation in *TAB2* (Table 1; Figure 1A, right panel). The presentation of subject 07 with the p.Gly168Arg TAK1 substitution is, however, milder than that of the rest of the cohort. Individuals 18 and 19 (p.Glu70Gln and p.Val100Glu, respectively) have a typical facial appearance for FMD; however, the skeletal presentation is milder (Table 1). Only individuals with the TAK1 p.Pro485Leu substitution developed keloid scarring (Table 1).

Altogether, we found four variants in *MAP3K7* to be causative of FMD in a total of 18 individuals. In the single remaining individual in this cohort, a missense mutation was identified in *TAB2,* which encodes for a protein that interacts directly with TAK1, the protein specified by *MAP3K7*.

TAK1 and *TAB2* Mutations Predict Substitutions in Functionally Relevant Conserved Domains

Our genetic studies identified five different missense mutations affecting two proteins that form part of the TAK1 complex. *MAP3K7* encodes TAK1, a MAP-3 kinase and the core enzymatic component of a multiprotein complex that is a hub for the control of many signaling pathways.[25] *TAB2* encodes TAB2, a scaffolding protein necessary for the activation of some of signaling properties of TAK1,[22] although it has not been shown to possess enzymatic activity itself.

TAK1 is comprised of an N-terminal kinase domain, a poorly characterized linker region, and a C-terminal coiled-coil domain[25,26] (Figure 2). Pro485 in TAK1, which is substituted to a leucine in 15 unrelated individuals with FMD, is phylogenetically highly conserved and the residue is invariant in both vertebrates and invertebrates, including *C. elegans* (genomic evolutionary rate profiling [GERP] score of 5.79, Figure 2A). The substitution occurs within the C terminus of TAK1 immediately N-terminal to the coiled-coil domain within a region that mediates interactions with TAB2[27] and that might also constitute a homodimerization interface[28] (Figure 2B). A crystal structure is available for the N-terminal kinase domain[29] but not for the linker region or C terminus, and therefore the structural consequences of substituting Pro485 cannot be ascertained. Variant effect prediction software (PolyPhen-2, MutationTaster, and SIFT) estimates that the recurrent p.Pro485Leu substitution is likely to be deleterious (PolyPhen score of 0.992, probably damaging; MutationTaster score of 0.999, disease causing; SIFT score of 0, damaging).

Similarly, the p.Glu70Gln, p.Val100Glu, and p.Gly168Arg substitutions lie within a stretch of 120 almost completely conserved residues in seven vertebrates. A glutamine at position 70 is conserved to *Drosophila* (GERP score, 5.22), and a valine at position 100 is conserved in the seven vertebrate homologs analyzed (GERP score, 5.67; Figure 2A). Both are predicted to be disease causing and have PolyPhen scores of 0.995 and 0.951, respectively (probably damaging), MutationTaster scores of 0.999 (disease causing), and SIFT scores of 0 (damaging). A glycine at position 168 is conserved in *Drosophila* (GERP score, 5.18; Figure 2A). PolyPhen (0.802, possibly damaging), MutationTaster (0.999, disease causing), and SIFT (0, damaging) predict this substitution to be disease causing. These three substitutions lie within the conserved kinase domain of TAK1 (Figure 2B). Predictions based on the published crystal structure[29] (TAK1-TAB1 fusion protein [PDB: 2EVA]) of this region of the protein suggest that the p.Gly168Arg substitution would disrupt a tightly constrained β-hairpin turn that is required to order the active site of the kinase domain (Figure 2C). Glu70 is close to an important loop that sits over the active site of the TAK1 enzyme; however, substitution to a glutamine is conservative and it might establish similar interactions within the structure. Val100 is located in a hydrophobic pocket with Ile65, Phe74, Arg71, and Leu97, and substitution to a glutamic acid could be destabilizing to this region (Figure 2C).

Prediction of the effect of the TAB2 variant (p.Glu569Lys) is constrained by limited data on this protein. The substitution has a PolyPhen-2 score of 0.989 (probably damaging), a MutationTaster score of 0.999 (disease causing), and a SIFT score of 0 (damaging), suggesting the potential for pathogenicity. Glu569 lies in an area of high conservation in vertebrates (GERP score, 5.06; Figure 2A), but no tertiary structure for this protein is available. Similar to TAK1, TAB2 has a C-terminal coiled-coil domain within which the TAK1 binding domain resides.[22,27] The p.Glu569Lys substitution is located five

Please cite this article in press as: Wade et al., Mutations in *MAP3K7* that Alter the Activity of the TAK1 Signaling Complex Cause Frontometaphyseal Dysplasia, The American Journal of Human Genetics (2016), http://dx.doi.org/10.1016/j.ajhg.2016.05.024

Table 1. Clinical and Radiographic Characteristics of Individuals with FMD

		Clinical Features							
Subject	Sex	Supraorbital Ridges	Small Chin	Hearing Loss	Hypertelorism	Downslanting Palpebral Fissures	Wide Nasal Bridge	Cleft Palate/Bifid Uvula[a]	Congenital Stridor/Subglottic Stenosis
01	M	+	+	+	+	+	+	–	+
02	M	+	+	+	+	+	+	+	+
03	M	+	–	+	+	+	+	–	U
04	M	+	–	+	+	+	+	U	U
05	M	+	+	+	+	+	+	–	–
06	M	+	+	U	+	+	+	–	–
07	M	+	–	–	+	–	+	–	–
08[b]	M	+	+	+	+	–	+	–	+
09	F	+	+	+	+	+	+	+	–
10[b]	F	+	+	+	+	+	+	–	–
11[b]	F	+	–	+	+	+	+	–	+
12	F	+	+	+	+	+	+	+	+
13[b]	F	+	+	+	+	+	+	+	+
14	F	+	+	U	+	+	+	–	U
15	F	+	+	+	+	+	+	+	–
16[b]	F	+	+	+	+	+	+	–	–
17	F	+	+	+	+	+	+	–	–
18[b]	F	+	+	+	+	+	+	–	U
19	F	+	+	–	+	+	+	–	–

+, present; −, absent; (+), equivocal; U, unknown; M, male; F, female.
[a]Including submucous cleft palate.
[b]Reported in Basart et al.[17] or Morava et al.[18].

residues N-terminal to this mapped TAK1 binding interface (residues 574–693, Figure 2B).

To evaluate the consequences of the recurrent *MAP3K7* c.1454C>T mutation at the level of the transcript, cDNA was prepared from cultured primary fibroblasts obtained from subjects 02, 13, and 16 (*MAP3K7* c.1454C>T) and RT-PCR followed by Sanger sequencing was performed. Sequence chromatograms demonstrated the persistence of the mutant allele in all instances and no additional RT-PCR products were observed (data not shown). An RNA source for subjects 07, 17, 18, and 19 was not available to test these alternative mutations in a similar manner. Together, these genetic, bioinformatic, and phylogenetic data constitute conclusive evidence that mutations in *MAP3K7* cause frontometaphyseal dysplasia.

To explore the mechanism by which mutations confer this phenotype, we first considered a hypothesis that invokes haploinsufficiency for the pathogenesis of this form of FMD. Individuals with haploinsufficiency encompassing the *MAP3K7* locus[30] and mice with conditional knockout of *Map3k7* in the skeleton do not have an osteosclerotic phenotype,[31,32] suggesting that the phenotype arising from the *MAP3K7* mutations described here is not a result of haploinsufficiency. To further test the hypothesis that the mutations in *MAP3K7* do not exhibit their pathogenic effect by affecting the stability of TAK1, we performed quantitative western blots on lysates prepared from cycloheximide-treated cells transfected with expression constructs specifying either WT TAK1 ($TAK1^{WT}$) or TAK1 with the p.Pro485Leu ($TAK1^{p.Pro485Leu}$) or the p.Gly168Arg ($TAK1^{p.Gly168Arg}$) substitutions. There was no difference in protein stability between mutant TAK1 and WT protein up to 8 hr after cycloheximide treatment (Figure 2D), indicating that the pathogenic effect of these alleles is unlikely to relate to destabilization of the protein product. Similarly, individuals with haploinsufficiency of *TAB2* have no skeletal dysplasia and instead present with cardiac malformations,[33] and *Tab2*-knockout mice die in utero of liver degeneration.[34] These data therefore suggest that the phenotype of the individual described here with a missense mutation at this locus is unlikely to arise from a haploinsufficient mechanism.

Please cite this article in press as: Wade et al., Mutations in *MAP3K7* that Alter the Activity of the TAK1 Signaling Complex Cause Frontometaphyseal Dysplasia, The American Journal of Human Genetics (2016), http://dx.doi.org/10.1016/j.ajhg.2016.05.024

				Radiological Features					
Hydronephrosis	**Scoliosis**	**Intellectual Disability**	**Keloid**	**Cervical Vertebral Fusion**	**Elbow Contractures/ Dislocated Radial Head**	**Flared Metaphyses**	**Digital and Wrist Contractures**	**Under-modeled Phalanges**	**Broad Thumbs and Fingers**
+	+	–	–	+	+	+	+	+	+
–	+	+	–	+	+	+	+	+	+
U	+	+	–	U	+	U	+	U	+
U	U	–	–	U	+	U	+	U	U
–	+	–	+	–	+	+	+	+	+
–	+	+	–	–	+	+	+	+	+
–	(+)	–	–	+	+	–	+	+	–
–	+	–	+	+	+	+	+	+	+
–	–	–	+	+	+	+	+	+	+
–	+	–	+	+	+	+	+	+	+
–	+	–	+	+	+	+	+	+	+
–	–	(+)	–	U	+	U	+	U	+
–	+	–	+	–	+	+	+	+	+
U	U	–	–	+	+	U	+	U	+
–	–	–	+	–	+	+	+	+	+
+	+	–	+	+	+	+	+	+	+
–	+	–	–	–	+	+	+	+	+
U	+	–	–	–	U	–	–	+	U
–	+	–	–		+	+	+	U	(+)

The p.Pro485Leu Substitution Does Not Affect TAK1/TAB2 Binding or TAK1 Homodimerization

A parsimonious hypothesis for the mechanism leading to FMD in these individuals would be that causative mutations disrupt the interaction between TAK1 and TAB2 given that both the recurrent mutation and the substitution in TAB2 lie within (or very close to) the interface formed by both proteins.[27] We used competitive co-immunoprecipitation to examine the relative TAB2 binding affinity of p.Pro485Leu in the presence of $TAK1^{WT}$ by using a transient transfection protocol in HEK293FT cells. Two differentially tagged TAK1 proteins, with one construct specifying the p.Pro485Leu substitution and the other WT, were transfected alongside TAB2, and immunoprecipitation was performed to measure the relative ability of these proteins to bind TAB2. No significant difference is observed between $TAK1^{WT}$ and $TAK1^{p.Pro485Leu}$ in their ability to bind TAB2 ($p = 0.59$; unpaired t test, Figure 3A), indicating that this interaction is physically unimpaired by the presence of the p.Pro485Leu substitution in TAK1.

A second hypothesis relates to the possibility that TAK1 homodimerizes[28] and that this activity impacts regulation of the signaling functions of the TAK1 complex. The TAK1 homodimerization interface has been mapped within the coiled-coil domain to a region that is adjacent to, but not overlapping, Pro485.[28] We tested the capacity of $TAK1^{WT}$ to dimerize with $TAK1^{p.Pro485Leu}$ by using competitive co-immunoprecipitation. Again, no significant difference ($p = 0.37$; unpaired t test) is noted between the formation of $TAK1^{WT/WT}$ homodimers and $TAK1^{p.Pro485Leu/WT}$ heterodimers, suggesting that the p.Pro485Leu substitution does not impair this activity (Figure S2).

$TAK1^{p.Pro485Leu}$ and $TAK1^{p.Gly168Arg}$ Increase TAK1 Autophosphorylation

In the absence of a clear mechanism relating the p.Pro485Leu substitution to mapped protein-protein interactions within the C terminus of TAK1, we sought evidence that this substitution altered the kinase activity of this protein. Upon activation, TAK1 is sequentially autophosphorylated within its kinase domain,[35] starting at Ser192 and followed by Thr178, Thr187, and Thr184, which in turn triggers the phosphorylation of a number of downstream effectors.[35–37] In addition to being scaffolded by

Please cite this article in press as: Wade et al., Mutations in *MAP3K7* that Alter the Activity of the TAK1 Signaling Complex Cause Frontometaphyseal Dysplasia, The American Journal of Human Genetics (2016), http://dx.doi.org/10.1016/j.ajhg.2016.05.024

Table 2. Mutations in *MAP3K7* and *TAB2*, Paternal Age at Birth, and Ancestry of Individuals with FMD

Subject	Gene	DNA	Protein	Inheritance	Paternal Age at Birth of Proband (Years)[a]	Ancestry
01	*MAP3K7*	c.1454C>T	p.Pro485Leu	de novo	33	Italian
02	*MAP3K7*	c.1454C>T	p.Pro485Leu	de novo	40	English
03	*MAP3K7*	c.1454C>T	p.Pro485Leu	U	36	Austrian
04	*MAP3K7*	c.1454C>T	p.Pro485Leu	U	38	Australian-European
05	*MAP3K7*	c.1454C>T	p.Pro485Leu	de novo	26	Scottish
06	*MAP3K7*	c.1454C>T	p.Pro485Leu	U	32	Swiss
08	*MAP3K7*	c.1454C>T	p.Pro485Leu	U	28	Korean
09	*MAP3K7*	c.1454C>T	p.Pro485Leu	U	18	Hispanic
10	*MAP3K7*	c.1454C>T	p.Pro485Leu	U	46	Turkish
11	*MAP3K7*	c.1454C>T	p.Pro485Leu	U	47	Mexican
12	*MAP3K7*	c.1454C>T	p.Pro485Leu	de novo	35	German
13	*MAP3K7*	c.1454C>T	p.Pro485Leu	U	26	English
14	*MAP3K7*	c.1454C>T	p.Pro485Leu	de novo	41	German
15	*MAP3K7*	c.1454C>T	p.Pro485Leu	U	30	Dutch
16	*MAP3K7*	c.1454C>T	p.Pro485Leu	de novo	40	Australian-European
18	*MAP3K7*	c.208G>C	p.Glu70Gln	dominant	U	French-Canadian
19	*MAP3K7*	c.299T>A	p.Val100Glu	dominant	U	Hungarian
07	*MAP3K7*	c.502G>C	p.Gly168Arg	de novo	28	Brazilian
17	*TAB2*	c.1705G>A	p.Glu569Lys	de novo	U	Australian-European

U, unknown.
[a]Mean, 34.4 and SD, 7.9.

TAB2, signaling through the TAK1 complex is also dependent on a second interacting factor, TAB1 (TAK1-associated binding protein 1 [MIM: 602615]).[26] To test whether the mutations leading to FMD affect TAK1 autophosphorylation, *MAP3K7* constructs specifying $TAK1^{WT}$, $TAK1^{p.Pro485Leu}$, and $TAK1^{p.Gly168Arg}$ were expressed in HEK293FT cells alongside constructs encoding its activating proteins TAB1 and TAB2. Under these conditions, quantitative western analysis revealed that both $TAK1^{p.Pro485Leu}$ and $TAK1^{p.Gly168Arg}$ are significantly more phosphorylated at Thr187 than $TAK1^{WT}$ ($p = 0.00014$ and $p = 0.00010$ respectively; unpaired t tests; Figure 3B). Consistent with the established facultative requirement for the co-activator TAB1 in mediating TAK1 autophosphorylation, no difference in the phosphorylation of TAK1 mutants was observed when TAK1 was expressed with TAB2 alone (Figure S3A).

The p.Pro485Leu Substitution Alters Signaling Downstream of the TAK1 Complex

Enhanced autophosphorylation of TAK1 in the presence of substitutions that lead to FMD suggests that signaling pathways downstream of this complex should exhibit altered activity. Multiple signaling pathways are activated downstream of TAK1, including JNK,[38] p38 MAPK,[39] and NF-κB[40] (Figure 4A). We first employed a luciferase reporter assay (Pathdetect, Agilent) that measures a global readout for transcriptional activation mediated by several MAPK targets, including ERK, p38, and JNK. A significantly enhanced activation of the reporter is observed for $TAK1^{p.Pro485Leu}$ in comparison to $TAK1^{WT}$ (Figure 4B). Given that this reporter system detects activity mediated via a number of MAPK pathway effectors, and considering the documented specific role for p-p38 downstream of TAK1 in the maintenance of bone mineralization in the mouse,[31] p-p38 was also assayed by western blot (Figure 4C). These data indicate that the $TAK1^{p.Pro485Leu}$ construct results in a substantial increase in phosphorylation of p38 compared to that mediated by $TAK1^{WT}$. Notably however, neither MAPK signaling nor p-p38 are increased when $TAK1^{p.Gly168Arg}$ is expressed under the same experimental conditions (Figures 4B and 4C), despite the significant increase in autophosphorylation noted in $TAK1^{p.Gly168Arg}$.

The second signaling pathway relevant to skeletogenesis that we evaluated was that mediated by NF-κB.[32,41] NF-κB is essential for RANK-L-mediated osteoclast differentiation,[42,43] whereas its activation inhibits osteoblastogenesis.[41] We used a luciferase reporter sensitive to activation of this pathway and found that both the

Please cite this article in press as: Wade et al., Mutations in *MAP3K7* that Alter the Activity of the TAK1 Signaling Complex Cause Frontometaphyseal Dysplasia, The American Journal of Human Genetics (2016), http://dx.doi.org/10.1016/j.ajhg.2016.05.024

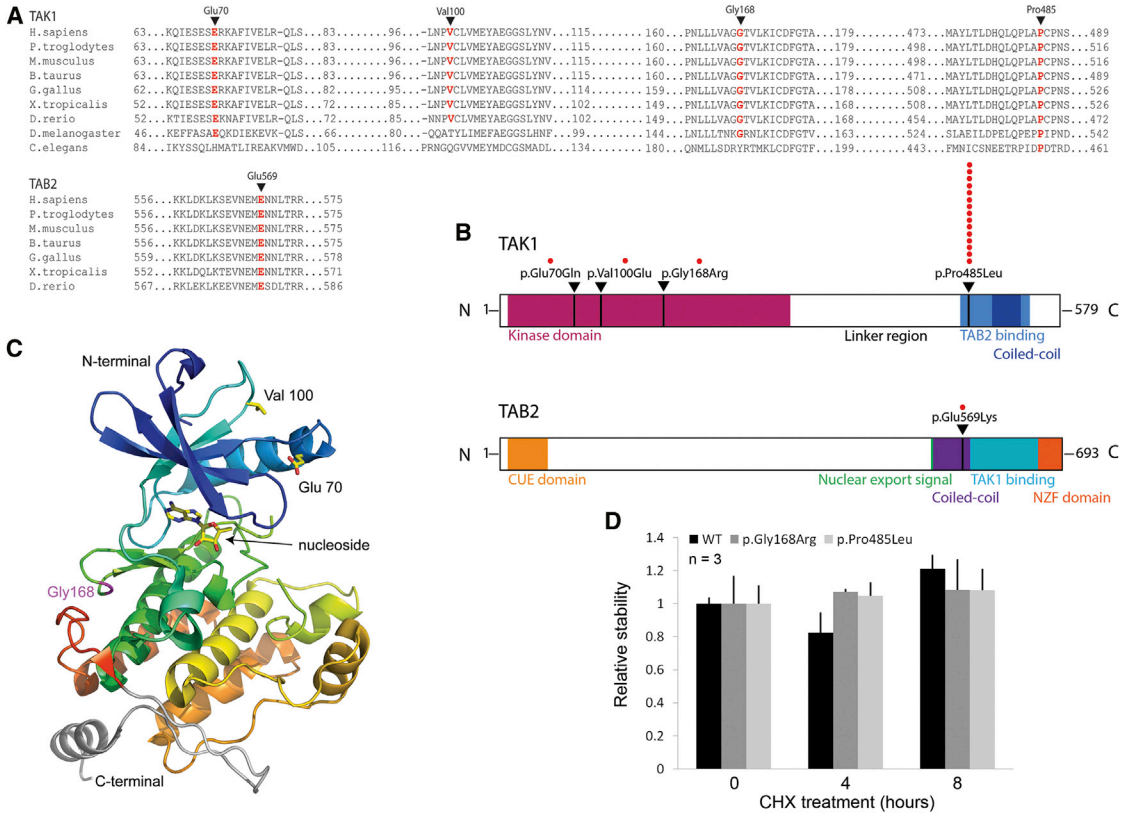

Figure 2. Conservation and Structural Consequences of Substitutions in TAK1 and TAB2

(A) The residues mutated in FMD2 are conserved to *C. elegans* at TAK1^{Pro485}, to *D. melanogaster* at TAK1^{Glu70} and TAK1^{Gly168}, and to zebrafish at TAK1^{Val100} and TAB2^{Glu569}. Sequences were obtained from the Ensembl Genome browser and aligned with Clustal Omega (European Bioinformatics Institute).

(B) All five substitutions are found within regions of functional significance; p.Glu70Gln, p.Val100Glu, and p.Gly168Arg are located in the middle of the kinase domain (magenta), p.Pro485Leu is located within the TAB2 binding domain on TAK1 (light blue), and p.Gly569Lys is within the coiled-coil domain, of TAB2, which is within the region mapped as critical for TAK1 binding.[27]

(C) Crystal structure for the N-terminal 303 amino acids of TAK1; Gly^{168} is located within a tight β-hairpin turn. Substitution to an arginine at this site has the potential to disrupt the kinase domain. Glu70 is close to a peptide loop that sits over the active site of the TAK1 enzyme, and substitution to a glutamine is conservative. Val100 is located in a hydrophobic pocket along with Ile65, Phe74, Arg71, and Leu97, and substitution to a glutamic acid could be destabilizing to this region.

(D) TAK1$^{p.Pro485Leu}$ and TAK1$^{p.Gly168Arg}$ do not alter the stability of TAK1 when normalized to TAK1^{WT} up to 8 hr after cycloheximide treatment of transfected cells.

Error bars show SD.

TAK1$^{p.Pro485Leu}$ and the TAK1$^{p.Gly168Arg}$ (Figure 4D) substitutions confer significantly reduced reporter activity in a transient transfection assay (Figure 4D). Together, these results indicate that signaling emanating from the TAK1 complex is altered by TAK1$^{p.Pro485Leu}$, but that the degree and quality of this disturbance is not exactly mirrored by the TAK1$^{p.Gly168Arg}$ substitution even though both variants enhance the autophosphorylation of the enzyme and the phenotypic consequences in the subjects with these variants are similar.

The p.Glu569Lys Substitution in TAB2 Alters MAPK Signaling

The observation of a single instance of a de novo missense variant in *TAB2* in an individual with FMD does not, in itself, constitute sufficiently strong evidence for pathogenicity. However, the location of this variant close to the mapped binding interface for TAB2 and TAK1 in an individual who demonstrates a phenotype that is indistinguishable from individuals with *MAP3K7*-associated FMD presents a strong a priori case for further investigation. We first questioned whether equivalent alterations to those observed in expression assays using the TAK1$^{p.Pro485Leu}$ construct in signaling were conferred by the de novo mutation in *TAB2*. We found that the presence of the TAB2$^{p.Glu569Lys}$ substitution alters neither TAK1 autophosphorylation (Figure 3B) nor NF-κB signaling activity (Figure 4D). There is, however, a clear increase in MAPK luciferase reporter activity and an increased p-p38/p38 ratio (Figures 4B and 4C), indicating that, despite a lack of enhanced autophosphorylation of TAK1, this variant in TAB2 has a strong effect on the activity of downstream components of the MAPK pathway.

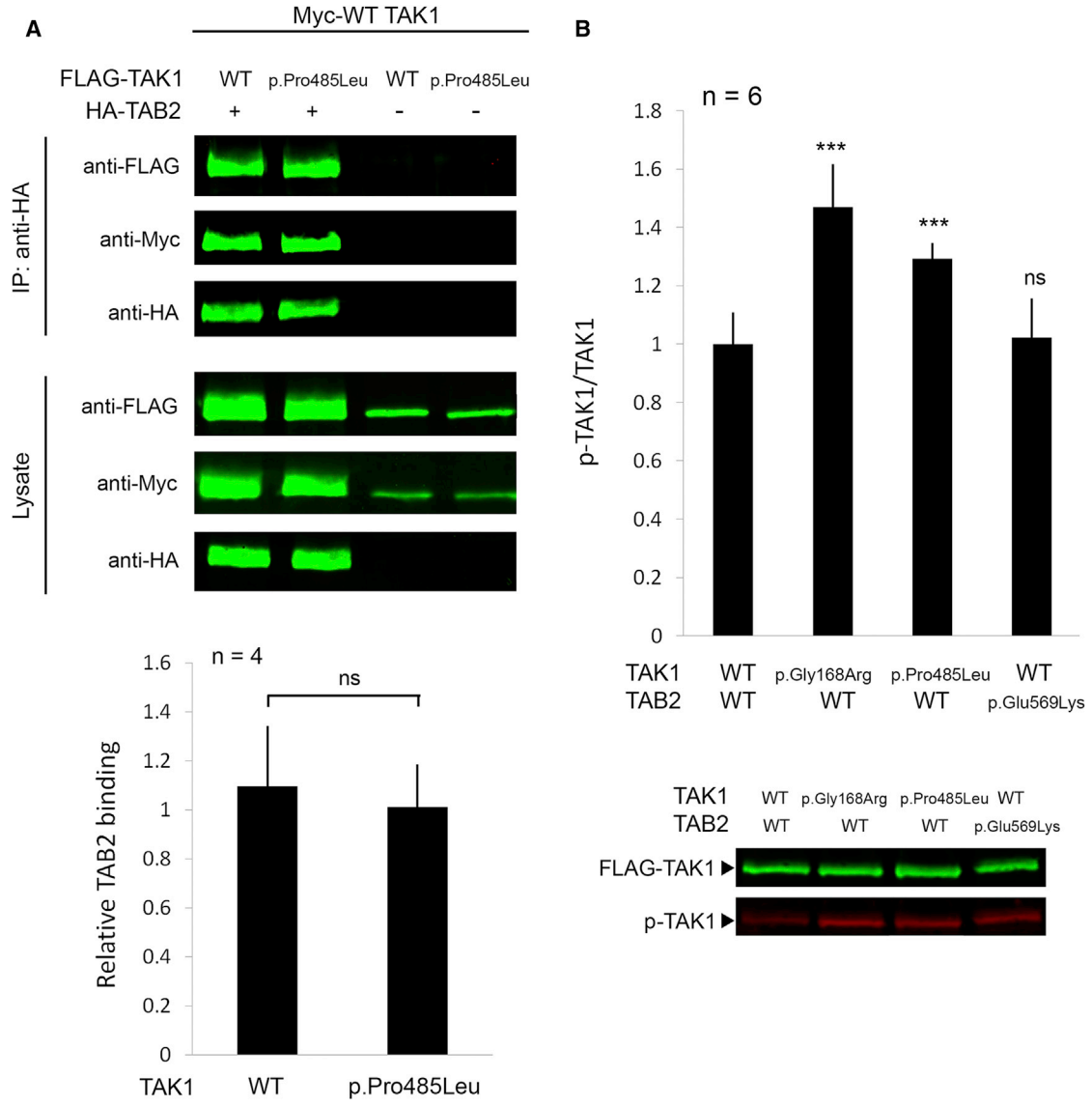

Figure 3. The Recurrent TAK1^{Pro485Leu} Substitution Does Not Impair TAB2 Binding but Increases Autophosphorylation of TAK1
(A) Competitive co-immunoprecipitation between FLAG-TAK1^{WT} or FLAG-TAK1$^{p.Pro485Leu}$ and HA-TAB2 shows no significant difference between TAK1^{WT} and TAK1$^{p.Pro485Leu}$ in terms of their ability to bind TAB2 in the presence of TAK1^{WT}.
(B) When expressed in HEK293FT cells, TAK1$^{p.Pro485Leu}$ and TAK1$^{p.Gly168Arg}$ have significantly increased phosphorylation when expressed with TAB1 and TAB2^{WT} in comparison to TAK1^{WT}. In contrast, when TAK1^{WT} is expressed with TAB1 and TAB2$^{p.Glu569Lys}$, there is no increased phosphorylation of TAK1. Detection of FLAG was used for the quantification of TAK1.
Error bars show SD.

Other Substituting Residues at TAK1 Pro485 Alter TAK1 Activity

Clinically, only the proline to leucine substitution is observed at position 485 in TAK1 in this cohort of individuals with FMD. Other mutations at this codon, however, might occur and lead to similar biochemical and clinical consequences. The likelihood of this might be dependent on the mode of gain of function and whether this primarily relates to the substitution of Pro485 and/or the identity of the substituting residue. We therefore examined the effect of other substitutions at the Pro485 codon to test the possibility that they might also confer a gain of function. Both p.Pro485Arg and p.Pro485Ala substitutions did enhance autophosphorylation (Figure S3B) and also had a variable effect on luciferase-based reporter assays for MAPK and NF-κB transcriptional targets. Substitution to an amino acid with a bulky and/or charged side chain (p.Pro485Arg) conferred more alteration in these signaling pathways than more conservative missense substitutions (e.g., p.Pro485Ala and p.Pro485Ser). Although TAK1$^{p.Pro485Arg}$ shows no increase in MAPK activity (Figure S4A), it does show a significant increase in p-p38 when measured on immunoblot, in addition to significantly decreased NF-κB activity (Figures S4B and S4C). Substitutions to residues with smaller and less polar side chains (Ser and Ala) result

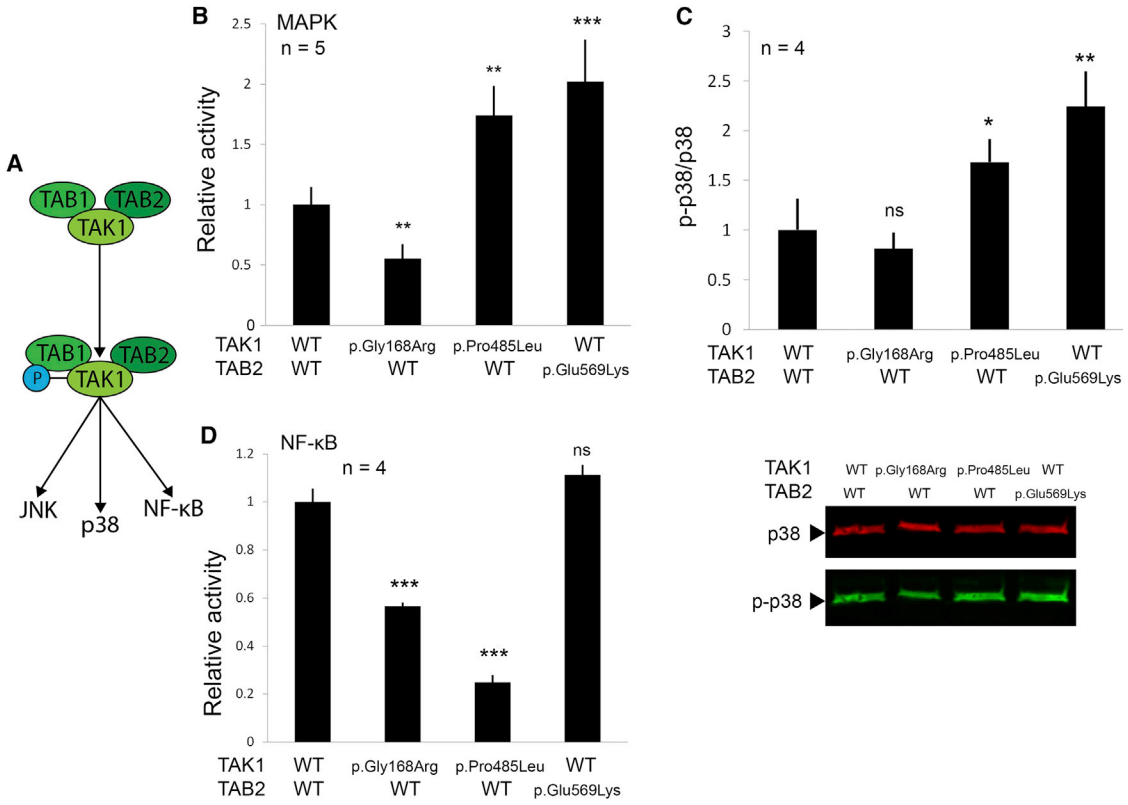

Figure 4. Both MAPK and NF-κB Signaling Activity Are Altered by TAK1 and TAB2 Substitutions
(A) Activated TAK1 has the ability to activate numerous downstream pathways, including those leading to the activation of the kinases JNK and p38, and the pro-inflammatory transcription factor NF-κB.
(B and C) Luciferase reporter for MAPK activity (B) and an immunoblot for phosphorylated-p38 (C), demonstrating that both $TAK1^{p.Pro485Leu}$-$TAB2^{WT}$ and $TAK1^{WT}$-$TAB2^{p.Glu569Lys}$ combinations are associated with significantly more activated MAPK in comparison to combinations of WT constructs in HEK293 cells. $TAK1^{p.Gly168Arg}$-$TAB2^{WT}$ is not significantly different from $TAK1^{WT}$-$TAB2^{WT}$.
(D) The activity of an NF-κB luciferase reporter showed that $TAK1^{p.Pro485Leu}$ and $TAK1^{p.Gly168Arg}$ have significantly reduced NF-κB activity in comparison to $TAK1^{WT}$, whereas $TAB2^{p.Glu569Lys}$ was no different than $TAK1^{WT}$ expressed with $TAB2^{WT}$.
Error bars show SD.

in no difference in signaling, as assayed either through reporter assays or p38 phosphorylation, except for a small but significant increase in p-p38 with $TAK1^{p.Pro485Ser}$ (Figure S4B). Overall, the changes in signaling function are smaller in magnitude to those conferred by the clinically observed substitution to leucine. We conclude that the identity of the substituting amino acid at this position does influence TAK1 function and that these substitutions also hold the potential to be disease causing.

Discussion

Until now, mutations in only one gene, *FLNA*, have been shown to cause FMD.[4] Here, we have used a combination of exome and targeted Sanger sequencing to reveal four mutations in *MAP3K7* to be the cause of FMD in 18 unrelated individuals and another variant in the gene encoding the interacting protein TAB2 to be likely causative of the condition in an additional individual. A specific mutation introducing a p.Pro485Leu substitution at the boundary of the C-terminal coiled-coil domain of the MAP-3 kinase, TAK1, was present in 15 unrelated individuals from diverse ethnic backgrounds. In all instances where parental samples were available (n = 6), this mutation had arisen de novo. A second de novo mutation predicting the substitution p.Gly168Arg was found in the highly conserved kinase domain of TAK1 in one individual. Two additional missense mutations leading to the substitutions p.Glu70Gln and p.Val100Glu, both inherited from a similarly affected parent, were found in another two subjects. We propose that the X-linked form of FMD be henceforth referred to as FMD1 to underscore its inheritance pattern and that the autosomal-dominant phenotype described here and caused by mutations in *MAP3K7*, the gene encoding TAK1, be denoted as FMD2. Although the de novo variant observed in TAB2 is an observation confined to a single individual, the functional relationship that this protein has with TAK1 and the biochemical activity it confers on the TAK1 signaling complex presents a strong, but still provisional, case that it also be considered causative of FMD. For this reason, we suggest that *TAB2* will eventually be shown to represent a third causative locus and that this form of FMD will be denoted as FMD3.

Phenotypically, there might be some differences between FMD1, FMD2, and *TAB2*-related FMD. Subjects with substitutions in the kinase domain of TAK1 have a notably milder phenotype than those with TAK1 p.Pro485Leu substitutions or *TAB2*- or *FLNA*- associated FMD, suggesting a phenotype-genotype correlation. We noted that the individuals with the recurrent substitution in TAK1 have a higher incidence of cleft palate (n = 5/16, or 31% of subjects, compared to 9% reported in FMD1).[3,17,44] We also previously reported a higher incidence of keloid scarring in individuals with FMD2 caused by TAK1$^{p.Pro485Leu}$.[17] This is notable because keloid is a rare phenotypic manifestation in Mendelian disorders, and the data presented here could increase the understanding of the pathogenesis of spontaneous keloid formation. Keloid might only very occasionally appear as a feature of FMD1,[3] but a recently described novel filaminopathy caused by a specific missense mutation in *FLNA* (c.4726G>A [p.Gly1576Arg] [GenBank: NM_001110556.1]) is also characterized by keloid scarring, joint contractures, and heart and kidney abnormalities. As such, it is reminiscent of FMD without its skeletal manifestations.[45,46] Therefore, it is possible that TAK1 and filamin A operate in the same pathway to promote keloid formation, a possibility consistent with data that indicate that activation of the TGF-β pathway, upstream of the MAP kinases p38, ERK, and JNK, has an important role in keloid pathogenesis. Small-molecule inhibition of p38, ERK, and JNK in cultured keloid fibroblasts impairs collagen accumulation and keloid development after TGFβ stimulation,[47] and therefore attention to therapeutic targets for keloid could usefully be focused on the pathway that links filamin A, TAK1, TGF-β, and MAP kinases.

FMD2 is primarily caused by TAK1$^{p.Pro485Leu}$ in the cohort presented here (15/18 individuals). The finding of a highly recurrent mutation is consistent with a gain-of-function mechanism. Although instances of highly recurrent mutations can be the result of a paternal-age effect,[48,49] we only demonstrated a modest signal for this once we tabulated the age of the fathers at the birth of the TAK1$^{p.Pro485Leu}$ individuals (Table 2).[48] A more salient observation is that the *MAP3K7* mutation occurs at a hypermutable CpG dinucleotide and therefore the observation of a C>T transition is expected to be more common than other mutations at this site.[50,51] We predict that other substitutions at the Pro485 codon will exist and be associated with FMD phenotypes, but these have not been identified in this study, perhaps because of an ascertainment bias or because of the small number of individuals studied here. It might be relevant to note that a less significant effect on downstream signaling is observed when Pro485 is replaced with residues other than leucine, and so if individuals do exist with alternative residues replacing Pro485, they might present with a milder phenotype.

The structural and biochemical reasons for why TAK1$^{p.Pro485Leu}$ is specifically implicated in this gain of function remain enigmatic. The TAK1$^{p.Pro485Leu}$ substitution does not impair TAB2 binding, homodimerization, or TAK1 stability. We note that Pro485 lies within a consensus sequence for prolyl hydroxylation (LXXLAP) as represented in other proteins,[52–54] but efforts to demonstrate that this site is subject to this form of modification by using mass spectroscopy, peptide substrates, and co-expression with prolyl hydroxylases failed to reveal any evidence to support this hypothesis (data not shown). Furthermore, substitution at this site with residues other than leucine did not invariably confer the same effect on autophosphorylation or signaling.

TAK1 is a MAP-3 kinase.[37] On activation, it binds its co-activators TAB1 and TAB2, leading to autophosphorylation, triggering downstream phosphorylation cascades.[37] The de novo TAK1 substitutions p.Pro485Leu and p.Gly168Arg significantly increase TAK1 autophosphorylation. The activated TAK1 complex is able to coordinate signaling in a number of different pathways, including the regulation of both osteoblast differentiation and activity.[31,55] The p38 pathway is especially critical because p38 phosphorylates and activates RUNX2, the master differentiation factor for osteoblasts, and DLX5, a transcription factor that stimulates the expression of the osteoblast genes *IBSP* (integrin-binding sialoprotein) and *SP7* (osterix).[31,55] TAK1$^{p.Pro485Leu}$ leads to increased phosphorylation of p38 and an enhanced ability to activate a generic MAPK transcriptional reporter. The TAK1$^{p.Gly168Arg}$ substitutions did not show the same ability to activate downstream MAPK cascades; this could reflect the noticeably milder phenotype in this individual and the lack of sensitivity of our assays to detect subtle changes in signaling outputs. The *TAB2* substitution p.Glu569Lys also increases MAPK signaling and enhances phosphorylation of p38, although these effects are not associated with activation of TAK1 via detectably enhanced autophosphorylation.

Not only is p38 essential for osteoblast differentiation,[31] it is also critical for the proper differentiation of osteoclasts in response to RANK-L.[56] Therefore a gain of function in p38 signaling in both cell types is predicted to result in both increased osteoblast differentiation and activity and increased osteoclast differentiation. Further evidence that p38 is a central, but not necessarily exclusive, mediator of TAK1-directed osteogenesis, is the observation that the osteopenia observed in mice with *Map3k7* deleted in the osteoblastic lineage is attributable to reduced p38 activation.[31]

The signaling output of TAK1 is complex and multifarious and also includes regulation of NF-κB.[57] Whereas MAPK signaling promotes the development of both the osteoblastic and osteoclastic lineage, NF-κB has opposing effects. Its activation by inflammatory cytokines is generally inhibitory for osteoblastogenesis[41,58] but essential for osteoclastogenesis stimulated by RANK and RANK-L.[42,43] Mice with an osteoclast-specific knockout of TAK1 have an osteopetrotic phenotype because of decreased NF-κB activation, demonstrating that TAK1 is necessary for proper osteoclast differentiation.[32] Reduced NF-κB

signaling could therefore promote hyperostosis by acting in concert in both of these cell types. Our data indicate that the TAK1$^{p.Pro485Leu}$ and TAK1$^{p.Gly168Arg}$ variants are associated with diminished NF-κB signaling, which is also the effect observed in an osteoclast-specific knockout of *Map3k7* in mice. Hence, we conclude that activity conferred by TAK1 substitutions cannot be attributed to a simple biochemical gain-of-function mechanism across all affected pathways given that it is clear that the TAK1-complex variants alter multiple outputs, in different directions. This could be especially important for TAK1$^{p.Gly168Arg}$, which does not increase MAPK signaling output but does decrease NF-κB activity. This could still, therefore, disrupt the overall ratio of MAPK to NF-κB signaling and cause a milder FMD phenotype. Additionally, our in vitro data indicate that the TAB2$^{p.Glu569Lys}$ substitution confers no difference in NF-κB signaling but still results in a florid FMD phenotype. Overall, this suggests that the combinatorial effect of these variants on all signaling pathways involved will likely only be definitively established once they can be evaluated in bone tissue from animal models of this disorder.

The TAB2$^{p.Glu569Lys}$ substitution does not increase TAK1 autophosphorylation, nor does it decrease NF-κB signaling output. TAB2 has a number of TAK1-independent functions, and therefore the phenotype arising from this substitution could be attributed to these activities. For instance, TAB2 has been shown to localize in the nucleus with transcriptional repressors N-CoR and HDAC3, where it acts to repress gene targets of NF-κB; the complex is exported out of the nucleus upon stimulation of the TAK1 complex.[59] Additionally, TAB2 has been shown to bind Smad7 downstream of TGF-β activation, which blocks TAK1-TAB2-TRAF2 complex assembly.[60] Taken together, these data suggest that TAB2 acts to repress signaling mediated by TAK1, but it is unknown whether TAB2 might also act to promote MAPK functions, although our results indicate that the Glu569Lys substitution does confer such activity.

As well as influencing major developmental mechanisms in the skeleton, TAK1 has a headline role governing the innate immune response and inflammation.[40] The TAK1 complex is activated by inflammatory cytokines (e.g., TNF-α[40] and IL-1[61]) and triggers downstream signaling responses to these stimuli, such as activation of NF-κB.[40,62] We expect that individuals with gain-of-function TAK1 signaling might present with inflammatory phenotypes; however, this is not a clinically apparent aspect of the FMD2 phenotype. Focused study from this point could reveal hitherto unexpected subclinical anomalies in this disorder.

The TAK1 signaling complex is a broadly dispersed signaling hub in multiple tissues. Our observation that alteration of its signaling functions via a specific mutational mechanism hints at levels of regulation of this complex that remain uncharacterized. Although the phenotype of FMD extends to tissues other than bone, the pronounced effect that these mutations have on the mineralization of the skeleton suggests that understanding the function of this signaling hub in this tissue could produce new insights and therapeutic options for conditions characterized by osteopenia.

Supplemental Data

Supplemental Data include four figures and four tables and can be found with this article online at http://dx.doi.org/10.1016/j.ajhg.2016.05.024.

Acknowledgments

The authors would like to thank the participating families and J. Weissenbach for diagnostic expertise. We thank K. Matsumoto for the kind gift of the TAB1 construct. The work was supported by funding from the Marsden Fund (S.P.R. and M.A.B.) and Cure Kids (S.P.R.). E.W. is supported by an Otago University postgraduate research scholarship, and A.M.L. is supported by a University of Queensland postgraduate scholarship (Australian Postgraduate Award). M.A.B. is funded by a National Health and Medical Research Council senior principal research fellowship.

Received: March 16, 2016
Accepted: May 22, 2016
Published: July 14, 2016

Web Resources

1000 Genomes, http://www.1000genomes.org
Burrows-Wheeler Aligner, http://bio-bwa.sourceforge.net/
Clustal Omega, http://www.ebi.ac.uk/Tools/msa/clustalo/
DECIPHER, http://decipher.sanger.ac.uk/
Ensembl Genome Browser, http://www.ensembl.org/index.html
ExAC Browser, http://exac.broadinstitute.org/
GATK, https://www.broadinstitute.org/gatk/
GenBank, http://www.ncbi.nlm.nih.gov/genbank/
GERP, http://mendel.stanford.edu/SidowLab/downloads/gerp/
MutationTaster, http://www.mutationtaster.org/
NHLBI Exome Sequencing Project (ESP) Exome Variant Server, ESP6500, http://evs.gs.washington.edu/EVS/
OMIM, http://www.omim.org/
Picard, http://broadinstitute.github.io/picard/
PolyPhen-2, http://genetics.bwh.harvard.edu/pph2/
RCSB Protein Data Bank, http://www.rcsb.org/pdb/home/home.do
SIFT, http://sift.bii.a-star.edu.sg/

References

1. Fitzsimmons, J.S., Fitzsimmons, E.M., Barrow, M., and Gilbert, G.B. (1982). Fronto-metaphyseal dysplasia. Further delineation of the clinical syndrome. Clin. Genet. *22*, 195–205.
2. Robertson, S.P., Twigg, S.R., Sutherland-Smith, A.J., Biancalana, V., Gorlin, R.J., Horn, D., Kenwrick, S.J., Kim, C.A., Morava, E., Newbury-Ecob, R., et al.; OPD-spectrum Disorders Clinical Collaborative Group (2003). Localized mutations in the gene encoding the cytoskeletal protein filamin A cause diverse malformations in humans. Nat. Genet. *33*, 487–491.
3. Robertson, S.P., Jenkins, Z.A., Morgan, T., Adès, L., Aftimos, S., Boute, O., Fiskerstrand, T., Garcia-Miñaur, S., Grix, A., Green, A., et al. (2006). Frontometaphyseal dysplasia: mutations in

FLNA and phenotypic diversity. Am. J. Med. Genet. A. *140*, 1726–1736.

4. Bonafe, L., Cormier-Daire, V., Hall, C., Lachman, R., Mortier, G., Mundlos, S., Nishimura, G., Sangiorgi, L., Savarirayan, R., Sillence, D., et al. (2015). Nosology and classification of genetic skeletal disorders: 2015 revision. Am. J. Med. Genet. A. *167A*, 2869–2892.
5. Foley, C., Roberts, K., Tchrakian, N., Morgan, T., Fryer, A., Robertson, S.P., and Tubridy, N. (2010). Expansion of the spectrum of *FLNA* mutations associated with Melnick-Needles syndrome. Mol. Syndromol. *1*, 121–126.
6. Robertson, S.P. (2007). Otopalatodigital syndrome spectrum disorders: otopalatodigital syndrome types 1 and 2, frontometaphyseal dysplasia and Melnick-Needles syndrome. Eur. J. Hum. Genet. *15*, 3–9.
7. Clark, A.R., Sawyer, G.M., Robertson, S.P., and Sutherland-Smith, A.J. (2009). Skeletal dysplasias due to filamin A mutations result from a gain-of-function mechanism distinct from allelic neurological disorders. Hum. Mol. Genet. *18*, 4791–4800.
8. Glogauer, M., Arora, P., Chou, D., Janmey, P.A., Downey, G.P., and McCulloch, C.A. (1998). The role of actin-binding protein 280 in integrin-dependent mechanoprotection. J. Biol. Chem. *273*, 1689–1698.
9. Loo, D.T., Kanner, S.B., and Aruffo, A. (1998). Filamin binds to the cytoplasmic domain of the β1-integrin: Identification of amino acids responsible for this interaction. J. Biol. Chem. *273*, 23304–23312.
10. Kim, H., and McCulloch, C.A. (2011). Filamin A mediates interactions between cytoskeletal proteins that control cell adhesion. FEBS Lett. *585*, 18–22.
11. Stossel, T.P., Condeelis, J., Cooley, L., Hartwig, J.H., Noegel, A., Schleicher, M., and Shapiro, S.S. (2001). Filamins as integrators of cell mechanics and signalling. Nat. Rev. Mol. Cell Biol. *2*, 138–145.
12. Gorlin, J.B., Yamin, R., Egan, S., Stewart, M., Stossel, T.P., Kwiatkowski, D.J., and Hartwig, J.H. (1990). Human endothelial actin-binding protein (ABP-280, nonmuscle filamin): a molecular leaf spring. J. Cell Biol. *111*, 1089–1105.
13. Baldassarre, M., Razinia, Z., Burande, C.F., Lamsoul, I., Lutz, P.G., and Calderwood, D.A. (2009). Filamins regulate cell spreading and initiation of cell migration. PLoS ONE *4*, e7830.
14. D'Addario, M., Arora, P.D., Ellen, R.P., and McCulloch, C.A. (2002). Interaction of p38 and Sp1 in a mechanical force-induced, β_1 integrin-mediated transcriptional circuit that regulates the actin-binding protein filamin-A. J. Biol. Chem. *277*, 47541–47550.
15. Gardel, M.L., Nakamura, F., Hartwig, J.H., Crocker, J.C., Stossel, T.P., and Weitz, D.A. (2006). Prestressed F-actin networks cross-linked by hinged filamins replicate mechanical properties of cells. Proc. Natl. Acad. Sci. USA *103*, 1762–1767.
16. Feng, Y., and Walsh, C.A. (2004). The many faces of filamin: a versatile molecular scaffold for cell motility and signalling. Nat. Cell Biol. *6*, 1034–1038.
17. Basart, H., van de Kar, A., Adès, L., Cho, T.-J., Carter, E., Maas, S.M., Wilson, L.C., van der Horst, C.M., Wade, E.M., Robertson, S.P., and Hennekam, R.C. (2015). Frontometaphyseal dysplasia and keloid formation without *FLNA* mutations. Am. J. Med. Genet. A. *167*, 1215–1222.
18. Morava, E., Illés, T., Weisenbach, J., Kárteszi, J., and Kosztolányi, G. (2003). Clinical and genetic heterogeneity in frontometaphyseal dysplasia: severe progressive scoliosis in two families. Am. J. Med. Genet. A. *116A*, 272–277.
19. McInerney-Leo, A.M., Schmidts, M., Cortés, C.R., Leo, P.J., Gener, B., Courtney, A.D., Gardiner, B., Harris, J.A., Lu, Y., Marshall, M., et al.; UK10K Consortium (2013). Short-rib polydactyly and Jeune syndromes are caused by mutations in WDR60. Am. J. Hum. Genet. *93*, 515–523.
20. Haack, T.B., Hogarth, P., Kruer, M.C., Gregory, A., Wieland, T., Schwarzmayr, T., Graf, E., Sanford, L., Meyer, E., Kara, E., et al. (2012). Exome sequencing reveals de novo WDR45 mutations causing a phenotypically distinct, X-linked dominant form of NBIA. Am. J. Hum. Genet. *91*, 1144–1149.
21. Dempsey, C.E., Sakurai, H., Sugita, T., and Guesdon, F. (2000). Alternative splicing and gene structure of the transforming growth factor β-activated kinase 1. Biochim. Biophys. Acta *1517*, 46–52.
22. Takaesu, G., Kishida, S., Hiyama, A., Yamaguchi, K., Shibuya, H., Irie, K., Ninomiya-Tsuji, J., and Matsumoto, K. (2000). TAB2, a novel adaptor protein, mediates activation of TAK1 MAPKKK by linking TAK1 to TRAF6 in the IL-1 signal transduction pathway. Mol. Cell *5*, 649–658.
23. Medina, M.T., Suzuki, T., Alonso, M.E., Durón, R.M., Martínez-Juárez, I.E., Bailey, J.N., Bai, D., Inoue, Y., Yoshimura, I., Kaneko, S., et al. (2008). Novel mutations in Myoclonin1/EFHC1 in sporadic and familial juvenile myoclonic epilepsy. Neurology *70*, 2137–2144.
24. Stogmann, E., Lichtner, P., Baumgartner, C., Bonelli, S., Assem-Hilger, E., Leutmezer, F., Schmied, M., Hotzy, C., Strom, T.M., Meitinger, T., et al. (2006). Idiopathic generalized epilepsy phenotypes associated with different EFHC1 mutations. Neurology *67*, 2029–2031.
25. Yamaguchi, K., Shirakabe, K., Shibuya, H., Irie, K., Oishi, I., Ueno, N., Taniguchi, T., Nishida, E., and Matsumoto, K. (1995). Identification of a member of the MAPKKK family as a potential mediator of TGF-β signal transduction. Science *270*, 2008–2011.
26. Shibuya, H., Yamaguchi, K., Shirakabe, K., Tonegawa, A., Gotoh, Y., Ueno, N., Irie, K., Nishida, E., and Matsumoto, K. (1996). TAB1: an activator of the TAK1 MAPKKK in TGF-β signal transduction. Science *272*, 1179–1182.
27. Besse, A., Lamothe, B., Campos, A.D., Webster, W.K., Maddineni, U., Lin, S.-C., Wu, H., and Darnay, B.G. (2007). TAK1-dependent signaling requires functional interaction with TAB2/TAB3. J. Biol. Chem. *282*, 3918–3928.
28. Ouyang, C., Nie, L., Gu, M., Wu, A., Han, X., Wang, X., Shao, J., and Xia, Z. (2014). Transforming growth factor (TGF)-beta-activated kinase 1 (TAK1) activation requires phosphorylation of serine 412 by protein kinase A catalytic subunit alpha (PKACa) and X-linked protein kinase (PRKX). J. Biol. Chem. *289*, 24226–24237.
29. Brown, K., Vial, S.C., Dedi, N., Long, J.M., Dunster, N.J., and Cheetham, G.M. (2005). Structural basis for the interaction of TAK1 kinase with its activating protein TAB1. J. Mol. Biol. *354*, 1013–1020.
30. Klein, O.D., Cotter, P.D., Moore, M.W., Zanko, A., Gilats, M., Epstein, C.J., Conte, F., and Rauen, K.A. (2007). Interstitial deletions of chromosome 6q: genotype-phenotype correlation utilizing array CGH. Clin. Genet. *71*, 260–266.
31. Greenblatt, M.B., Shim, J.-H., Zou, W., Sitara, D., Schweitzer, M., Hu, D., Lotinun, S., Sano, Y., Baron, R., Park, J.M., et al. (2010). The p38 MAPK pathway is essential for skeletogenesis and bone homeostasis in mice. J. Clin. Invest. *120*, 2457–2473.

32. Qi, B., Cong, Q., Li, P., Ma, G., Guo, X., Yeh, J., Xie, M., Schneider, M.D., Liu, H., and Li, B. (2014). Ablation of Tak1 in osteoclast progenitor leads to defects in skeletal growth and bone remodeling in mice. Sci. Rep. *4*, 7158.
33. Thienpont, B., Zhang, L., Postma, A.V., Breckpot, J., Tranchevent, L.C., Van Loo, P., Møllgård, K., Tommerup, N., Bache, I., Tümer, Z., et al. (2010). Haploinsufficiency of TAB2 causes congenital heart defects in humans. Am. J. Hum. Genet. *86*, 839–849.
34. Sanjo, H., Takeda, K., Tsujimura, T., Ninomiya-Tsuji, J., Matsumoto, K., and Akira, S. (2003). TAB2 is essential for prevention of apoptosis in fetal liver but not for interleukin-1 signaling. Mol. Cell. Biol. *23*, 1231–1238.
35. Scholz, R., Sidler, C.L., Thali, R.F., Winssinger, N., Cheung, P.C., and Neumann, D. (2010). Autoactivation of transforming growth factor β-activated kinase 1 is a sequential bimolecular process. J. Biol. Chem. *285*, 25753–25766.
36. Kishimoto, K., Matsumoto, K., and Ninomiya-Tsuji, J. (2000). TAK1 mitogen-activated protein kinase kinase kinase is activated by autophosphorylation within its activation loop. J. Biol. Chem. *275*, 7359–7364.
37. Dai, L., Aye Thu, C., Liu, X.-Y., Xi, J., and Cheung, P.C. (2012). TAK1, more than just innate immunity. IUBMB Life *64*, 825–834.
38. Akiyama, S., Yonezawa, T., Kudo, T.A., Li, M.G., Wang, H., Ito, M., Yoshioka, K., Ninomiya-Tsuji, J., Matsumoto, K., Kanamaru, R., et al. (2004). Activation mechanism of c-Jun amino-terminal kinase in the course of neural differentiation of P19 embryonic carcinoma cells. J. Biol. Chem. *279*, 36616–36620.
39. Wang, C., Deng, L., Hong, M., Akkaraju, G.R., Inoue, J., and Chen, Z.J. (2001). TAK1 is a ubiquitin-dependent kinase of MKK and IKK. Nature *412*, 346–351.
40. Takaesu, G., Surabhi, R.M., Park, K.-J., Ninomiya-Tsuji, J., Matsumoto, K., and Gaynor, R.B. (2003). TAK1 is critical for IkappaB kinase-mediated activation of the NF-kappaB pathway. J. Mol. Biol. *326*, 105–115.
41. Li, Y., Li, A., Strait, K., Zhang, H., Nanes, M.S., and Weitzmann, M.N. (2007). Endogenous TNFα lowers maximum peak bone mass and inhibits osteoblastic Smad activation through NF-kappaB. J. Bone Miner. Res. *22*, 646–655.
42. Udagawa, N., Takahashi, N., Jimi, E., Matsuzaki, K., Tsurukai, T., Itoh, K., Nakagawa, N., Yasuda, H., Goto, M., Tsuda, E., et al. (1999). Osteoblasts/stromal cells stimulate osteoclast activation through expression of osteoclast differentiation factor/RANKL but not macrophage colony-stimulating factor: receptor activator of NF-kappaB ligand. Bone *25*, 517–523.
43. Iotsova, V., Caamaño, J., Loy, J., Yang, Y., Lewin, A., and Bravo, R. (1997). Osteopetrosis in mice lacking NF-kappaB1 and NF-kappaB2. Nat. Med. *3*, 1285–1289.
44. Zenker, M., Nährlich, L., Sticht, H., Reis, A., and Horn, D. (2006). Genotype-epigenotype-phenotype correlations in females with frontometaphyseal dysplasia. Am. J. Med. Genet. A. *140*, 1069–1073.
45. Atwal, P., Blease, S., Braxton, A., Graves, J., He, W., Person, R., Slattery, L., Bernstein, J., and Hudgins, L. (2015). Novel X-linked syndrome of cardiac valvulopathy, keloid scarring, and reduced joint mobility due to filamin A substitution G1576R. Am. J. Med. Genet. A. *170*, 891–895.
46. Lah, M., Niranjan, T., Srikanth, S., Holloway, L., Schwartz, C., Wang, T., and Weaver, D. (2015). A distinct X-linked syndrome involving joint contractures, keloids, large optic cup-to-disc ratio, and renal stones results from a filamin A (FLNA) mutation. Am. J. Med. Genet. A *170*, 881–890.
47. He, S., Liu, X., Yang, Y., Huang, W., Xu, S., Yang, S., Zhang, X., and Roberts, M.S. (2010). Mechanisms of transforming growth factor β1/Smad signalling mediated by mitogen-activated protein kinase pathways in keloid fibroblasts. Br. J. Dermatol. *162*, 538–546.
48. Bray, I., Gunnell, D., and Davey Smith, G. (2006). Advanced paternal age: how old is too old? J. Epidemiol. Community Health *60*, 851–853.
49. Kong, A., Frigge, M.L., Masson, G., Besenbacher, S., Sulem, P., Magnusson, G., Gudjonsson, S.A., Sigurdsson, A., Jonasdottir, A., Jonasdottir, A., et al. (2012). Rate of *de novo* mutations and the importance of father's age to disease risk. Nature *488*, 471–475.
50. Cooper, D.N., and Krawczak, M. (1989). Cytosine methylation and the fate of CpG dinucleotides in vertebrate genomes. Hum. Genet. *83*, 181–188.
51. Rahbari, R., Wuster, A., Lindsay, S.J., Hardwick, R.J., Alexandrov, L.B., Al Turki, S., Dominiczak, A., Morris, A., Porteous, D., Smith, B., et al.; UK10K Consortium (2016). Timing, rates and spectra of human germline mutation. Nat. Genet. *48*, 126–133.
52. Ivan, M., Kondo, K., Yang, H., Kim, W., Valiando, J., Ohh, M., Salic, A., Asara, J.M., Lane, W.S., and Kaelin, W.G., Jr. (2001). HIFα targeted for VHL-mediated destruction by proline hydroxylation: Implications for O_2 sensing. Science *292*, 464–468.
53. Jaakkola, P., Mole, D.R., Tian, Y.-M., Wilson, M.I., Gielbert, J., Gaskell, S.J., von Kriegsheim, A., Hebestreit, H.F., Mukherji, M., Schofield, C.J., et al. (2001). Targeting of HIF-α to the von Hippel-Lindau ubiquitylation complex by O_2-regulated prolyl hydroxylation. Science *292*, 468–472.
54. Yu, F., White, S.B., Zhao, Q., and Lee, F.S. (2001). HIF-1α binding to VHL is regulated by stimulus-sensitive proline hydroxylation. Proc. Natl. Acad. Sci. USA *98*, 9630–9635.
55. Greenblatt, M.B., Shim, J.-H., and Glimcher, L.H. (2013). Mitogen-activated protein kinase pathways in osteoblasts. Annu. Rev. Cell Dev. Biol. *29*, 63–79.
56. Li, X., Udagawa, N., Itoh, K., Suda, K., Murase, Y., Nishihara, T., Suda, T., and Takahashi, N. (2002). p38 MAPK-mediated signals are required for inducing osteoclast differentiation but not for osteoclast function. Endocrinology *143*, 3105–3113.
57. Sakurai, H., Shigemori, N., Hasegawa, K., and Sugita, T. (1998). TGF-β-activated kinase 1 stimulates NF-κB activation by an NF-κB-inducing kinase-independent mechanism. Biochem. Biophys. Res. Commun. *243*, 545–549.
58. Chang, J., Wang, Z., Tang, E., Fan, Z., McCauley, L., Franceschi, R., Guan, K., Krebsbach, P.H., and Wang, C.Y. (2009). Inhibition of osteoblastic bone formation by nuclear factor-kappaB. Nat. Med. *15*, 682–689.
59. Baek, S.H., Ohgi, K.A., Rose, D.W., Koo, E.H., Glass, C.K., and Rosenfeld, M.G. (2002). Exchange of N-CoR corepressor and Tip60 coactivator complexes links gene expression by NF-kappaB and β-amyloid precursor protein. Cell *110*, 55–67.
60. Hong, S., Lim, S., Li, A.G., Lee, C., Lee, Y.S., Lee, E.-K., Park, S.H., Wang, X.-J., and Kim, S.-J. (2007). Smad7 binds to the adaptors TAB2 and TAB3 to block recruitment of the kinase TAK1 to the adaptor TRAF2. Nat. Immunol. *8*, 504–513.
61. Jiang, Z., Ninomiya-Tsuji, J., Qian, Y., Matsumoto, K., and Li, X. (2002). Interleukin-1 (IL-1) receptor-associated kinase-dependent IL-1-induced signaling complexes phosphorylate TAK1 and TAB2 at the plasma membrane and activate TAK1 in the cytosol. Mol. Cell. Biol. *22*, 7158–7167.
62. Hatada, E.N., Krappmann, D., and Scheidereit, C. (2000). NF-kappaB and the innate immune response. Curr. Opin. Immunol. *12*, 52–58.

The American Journal of Human Genetics, Volume *99*

Supplemental Data

Mutations in *MAP3K7* that Alter the Activity of the TAK1 Signaling Complex Cause Frontometaphyseal Dysplasia

Emma M. Wade, Philip B. Daniel, Zandra A. Jenkins, Aideen McInerney-Leo, Paul Leo, Tim Morgan, Marie Claude Addor, Lesley C. Adès, Debora Bertola, Axel Bohring, Erin Carter, Tae-Joon Cho, Hans-Christoph Duba, Elaine Fletcher, Chong A. Kim, Deborah Krakow, Eva Morava, Teresa Neuhann, Andrea Superti-Furga, Irma Veenstra-Knol, Dagmar Wieczorek, Louise C. Wilson, Raoul C.M. Hennekam, Andrew J. Sutherland-Smith, Tim M. Strom, Andrew O.M. Wilkie, Matthew A. Brown, Emma L. Duncan, David M. Markie, and Stephen P. Robertson

Supplemental Data

Figure S1

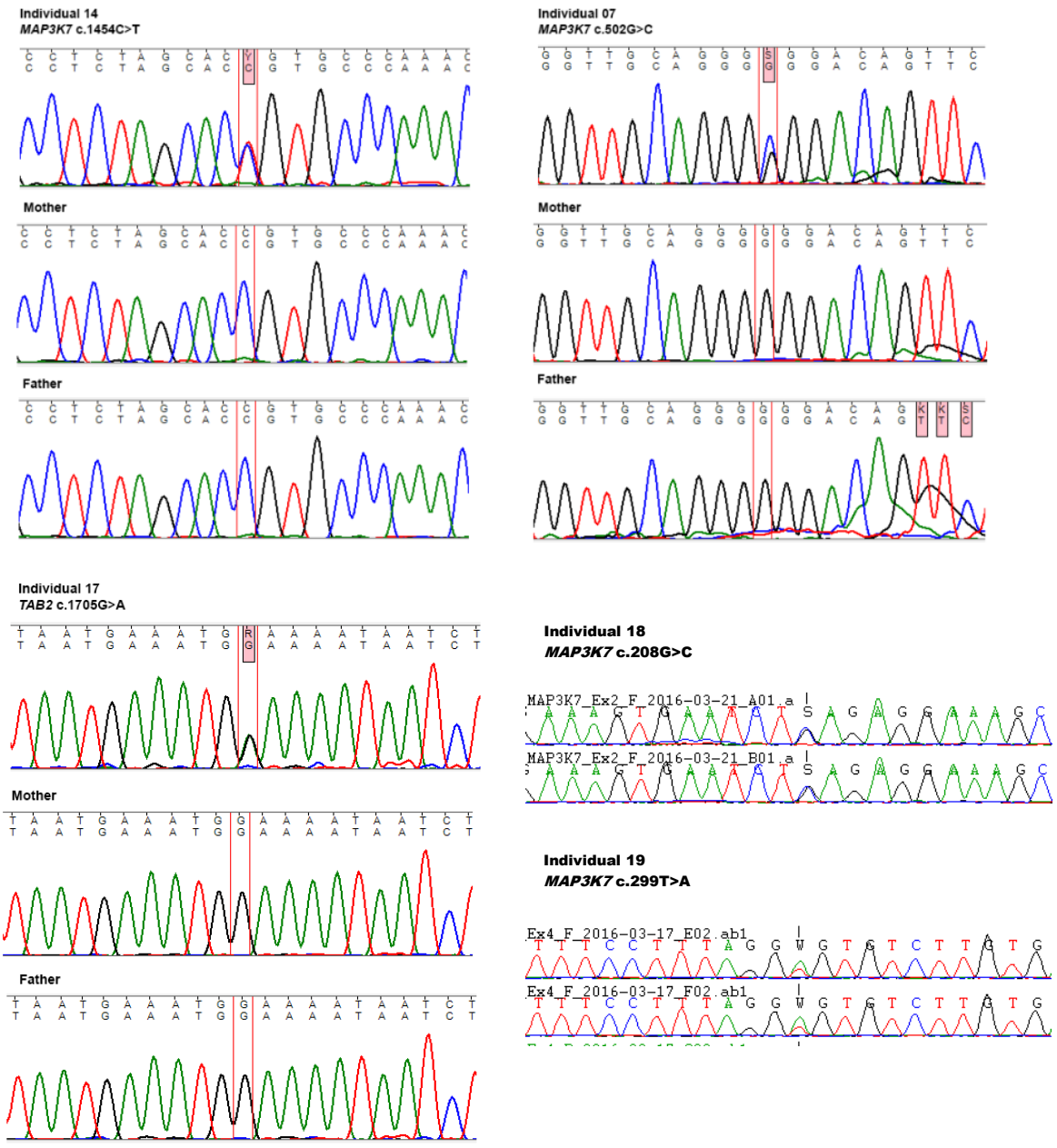

Figure S1. Chromatograms showing mutations in *MAP3K7* and *TAB2:* Chromatograms of individual 07 showing the heterozygous c.502G>C mutation in *MAP3K7*, and the parents who are homozygous for the reference allele; individual 14 showing the heterozygous c.1454C>T mutation in *MAP3K7*, and the parents who are both homozygous for the reference allele; individual 17 showing the heterozygous c.1705G>A mutation in *TAB2*, and the parents who are homozygous for the reference allele; individual 18 showing the heterozygous c.208C>T mutation in *MAP3K7;* and individual 19 showing the heterozygous c.299T>A mutation in *MAP3K7*. All parental relationships were confirmed with micro-satellite genotyping

Figure S2

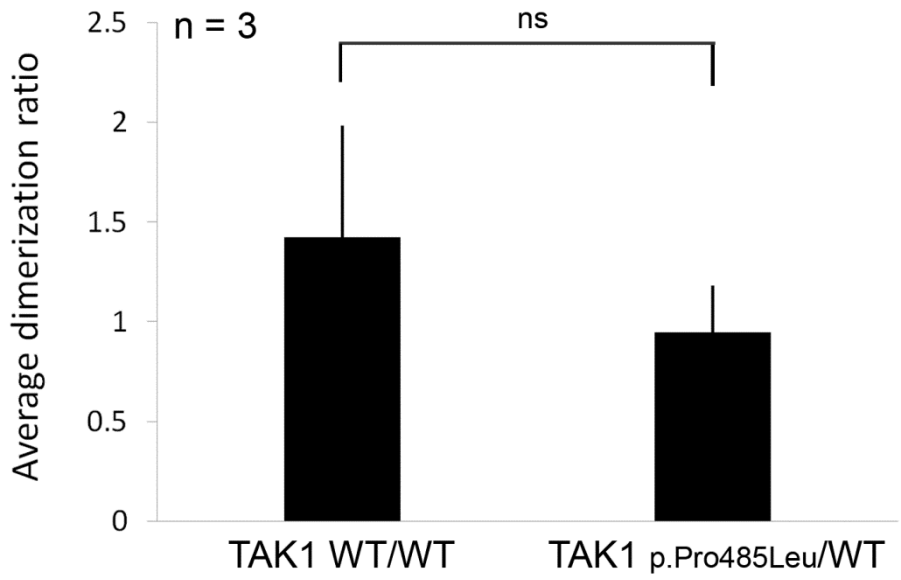

Figure S2. TAK1 dimerisation is not affected by TAK1$^{p.Pro485Leu}$: Competitive co-immunoprecipitation, in HEK293ft cells, showed that TAK1$^{p.Pro485Leu}$ did not have a significantly different capacity to homodimerise with TAK1^{WT} than TAK1^{WT} (unpaired t test, error bars show standard deviation)

Figure S3

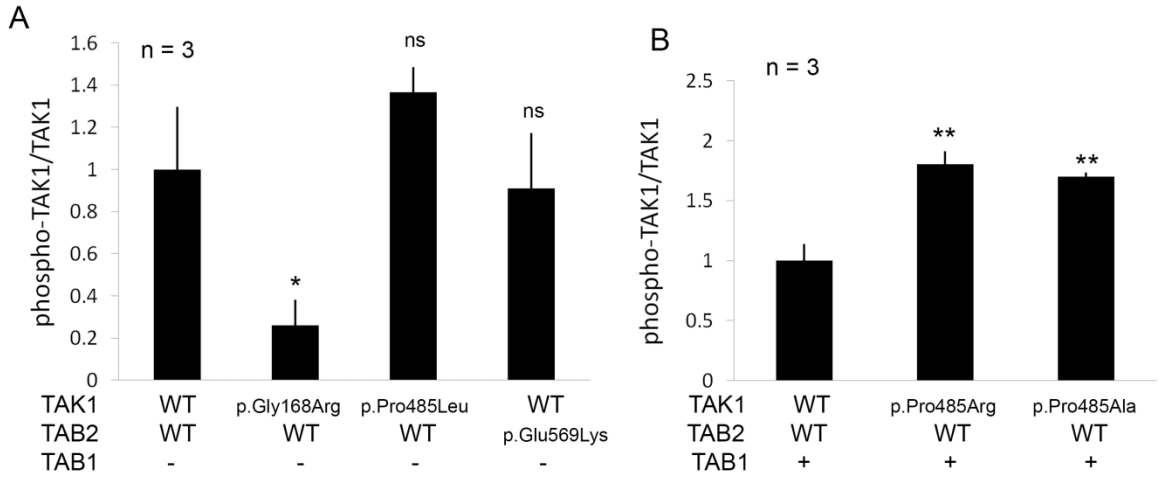

Figure S3. TAK1$^{p.Pro485Leu}$ increased phosphorylation is dependent on TAB2; in the presence of TAB2 other Pro485 positional mutants are hyperphosphorylated: (A) When co-expressed with TAB2^{WT}, and not TAB1, in HEK293ft cells TAK1$^{p.Pro485Leu}$ was not significantly more phosphorylated than TAK1^{WT}, also TAK1^{WT} was not more phosphorylated when co-expressed with TAB2$^{p.Glu569Lys}$, without TAB1. (B) The non-FMD2 causing Pro485 substitutions TAK1$^{p.Pro485Arg}$ and TAK1$^{p.Pro485Ala}$ are significantly more phosphorylated than TAK1^{WT} when expressed with TAB1 and TAB2^{WT} in HEK293ft cells (unpaired t tests, error bars show standard deviation)

Figure S4

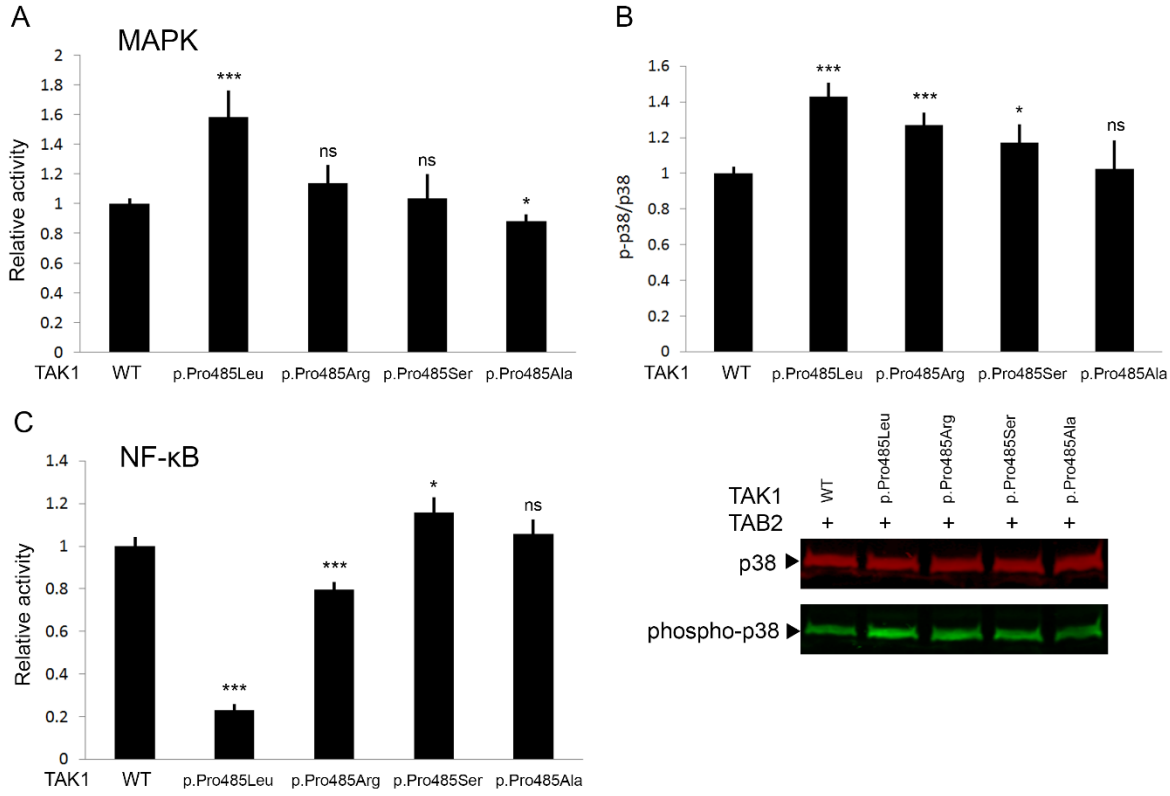

Figure S4: The effect on TAK1 signalling at Pro485 varies with the identity of the substituting residue. TAK1 constructs containing different substitutions at the 485 position were expressed alongside $TAB2^{WT}$ in HEK293 cells, (A) Only $TAK1^{p.Pro485Leu}$ significantly increases MAPK luciferase reporter activity however (B) a specific immunoblot to measure phosphorylated-p38 shows that $TAK1^{p.Pro485Arg}$ and $TAK1^{p.Pro485Ser}$ also have increased activity, although not as pronounced as that conferred by $TAK1^{p.Pro485Leu}$. $TAK1^{p.Pro485Ala}$ was not significantly different from $TAK1^{WT}$. (C) NF-κB luciferase reporter assay showing that $TAK1^{p.Pro485Arg}$ has decreased NF-κB activity compared to $TAK1^{WT}$ but this was not as reduced as $TAK1^{p.Pro485Leu}$. $TAK1^{p.Pro485Ser}$ has a small but significant increase in NF-κB activity and $TAK1^{p.Pro485Ala}$ is not significantly different from $TAK1^{WT}$. Error bars show standard deviation.

Table S1: Primer pairs used to sequence the exons of TAK1 and TAB2

Primer	Sequence	Primer	Sequence
TAK1 1F	GGAACCGGAAGTGTAGTGGG	TAB2 1F	AGGAGGAGGAGAGACAGAGG
TAK1 1R	CACTCCCACGTTACTGAGGG	TAB2 1R	AGGAGGCTGAATGAATGTAGGT
TAK1 2F	TGATTCCGATTCTTGTGGTGT	TAB2 2F	TCTTGTTCTGCCTACCTCTAGT
TAK1 2R	ACCGAATTGCTGATGTTCATGT	TAB2 2R	GGCAGTTACACAGGCTAAGC
TAK1 3F	CATTCTGGGCAGTCACTTGG	TAB2 3F	AAAGAATCTGGGAAGACAACCT
TAK1 3R	TGCCATGTCATTTCTCACAGG	TAB2 3R	CAGAAAGCTCCATCTTGCCA
TAK1 4F	TCACATAGTAGGGGCCAAAAGA	TAB2 4aF	AGCCAGTCACTTGGTAATCATG
TAK1 4R	TTTTGGGACTCTGACGGCA	TAB2 4aR	ACATGAGAGGTCTGGTGGC
TAK1 5F	AAGCAGGACTGATGGAGCAT	TAB2 4bF	ACCTCATCTCAACAGCCAAA
TAK1 5R	GAATTAGAGAGTGGGTTCGGG	TAB2 4bR	AACCATCCCACCTTTAGTATTCA
TAK1 6F	TGTTGGCCTTGTAACTTTTGATG	TAB2 5-6F	TTAAAGTGGGTGGGTCCTCA
TAK1 6R	ACAAGGAGTGAGGGAGATTATCA	TAB2 5-6R	GCCACAGAAAAACTGCTGGT
TAK1 7F	TCCCTGATACCCATTCTCAAAAT	TAB2 7F	AGGGGCAAAATAAATGAAAAGCA
TAK1 7R	TTAGGGAAGGGGACAGGAGT	TAB2 7R	AGAGAGGAAGGTTGCTGAAC
TAK1 8F	AGAGTTTGCATCATTCTTTGGGT	TAB2 8F	AAATGGTGTTTAAAGTTGCCTGT
TAK1 8R	CCCCTAAATCCAAAGCCCCT	TAB2 8R	AGAGAAGATACAGGGCCATTTG
TAK1 9F	TTCTTAGGTAGGTGCATGGC		
TAK1 9R	ATGAAGAATGACGCACCTGT		
TAK1 10F	CCTGCCTGGCTAGTTTATAAAAG	TAK1 cDNA F	GTGAGCAGTAGGTCATCCAGTCCCAGT
TAK1 10R	GCTCTTTTGCATGTTTCAGGA	TAK1 cDNA R	ATCATGAAGTGCCTTGTCGTTTC
TAK1 11F	CCCATTTGCCATCTTCCTCC		
TAK1 11R	TCACTCTTCAGACTTGTAGTTCC		
TAK1 12F	TCCGTGTTACTGTTTGTGGT		
TAK1 12R	TCATTATTCCGGTTCCACAGC		
TAK1 13F	GATCCAAGGAGCAACAAATTCC		
TAK1 13R	ACAGCGCTAATGAACAATTTACT		
TAK1 14F	GGATCTCTAAGTCTCTTCTTGCC		
TAK1 14R	GTATGAAGAAACAGACTGGTCAC		
TAK1 15F	TGGGGAGTTTGATTAGATAGGGT		
TAK1 15R	TTTAAGGAGGCCAACTAAAAGGA		
TAK1 16F	TCTGTCTTGACTCTCATCTTAGC		
TAK1 16R	AACTACGTTTTCATTGCACCTT		
TAK1 17F	GCTTCCATCATCAGCTACTAAGG		
TAK1 17R	GCATCAAAGCCCTTACACGG		

Number in primer name refers to target exon

Table S2: Primer pairs used to generate TAK1 and TAB2 expression constructs

Initial amplification primers – TAK1		
Pair 1 pcDNA3.1	F: TTCGAATTCGCGAGGGATCATGTCTACAG	R: CCGGGATCCCAGAGAATCATGAAGTGC
Pair 2 pCMV-Myc	F: TATGGCCATGGAGGCCCGATCTACAGCCTCTGCCGCCTCC	R: TCATGTCTGGATCCCCGCTCATGAAGTGCCTTGTCGTTTCTG
Pair 3 pCMV-HA	F: TATGGCCATGGAGGCCCGATCTACAGCCTCTGCCGCCTCCTC	R: AGAGATCTCGGTCGACCGTCATGAAGTGCCTTGTCGTTTCTG
Pair 4 p3xFLAG	F: GACAAGCTTGCGGCCGCGTCTACAGCCTCTGCCGCCTCC	R: GGATGCCACCCGGGATCCTTCATGAAGTGCCTTGTCGTTTCTG
Initial amplification primers – TAB2		
Pair 5 pCMV-HA	F: TATGGCCATGGAGGCCCGAGCCCAAGGAAGCCACCAAATTGAT	R: AGAGATCTCGGTCGACCGTCAGAAATGCCTTGGCATCTCACACTG
Mutagenesis primers		
TAK1 G168R	F: GTTGCAGGGCGGACAGTTCTAAAAATTTGTG	R: GAACTGTCCGCCCTGCAACCAGCAGTAAG
TAK1 P485L	F: CTCTAGCACTGTGCCCAAACTCCAAAGAATC	R: GTTTGGGCACAGTGCTAGAGGCTGTAGTTGG
TAK1 P485A	F: CTCTAGCAGCGTTGCCCAAACTCCAAAGAATC	R: GTTTGGGCACGCTGCTAGAGGCTGTAGTTGG
TAK1 P485R	F: CTCTAGCACGGTTGCCCAAACTCCAAAGAATC	R: GTTTGGGCACCGTGCTAGAGGCTGTAGTTGG
TAK1 P485S	F: CTCTAGCATCGTTGCCCAAACTCCAAAGAATC	R: GTTTGGGCACGATGCTAGAGGCTGTAGTTGG
TAB2 E569K	F: GTTAATGAAATGAAAAATAATCTAACTC	R: AGTTAGATTATTTTTCATTTCATTAACC

Table S3: Coverage and mapping data from individuals sequenced on the Agilent SureSelect Human All Exon V4+UTRs chip

Individual	Subject 01	Sibling 01	Mother 01	Father 01	Subject 02	Mother 02	Father 02	Subject 05	Mother 05	Father 05
Total reads	106,493,680	63,853,341	46,674,820	81,582,899	165,020,599	35,997,633	59,559,617	140,776,595	66,035,919	72,373,797
Mapped reads [a]	92,324,081 (86.69%)	55,982,531 (87.67%)	40,387,525 (86.53%)	71,863,933 (88.09%)	142,626,619 (86.43%)	30,337,637 (84.28%)	51,966,431 (87.25%)	121,754,108 (86.49%)	57,653,931 (87.31%)	63,579,562 (87.85%)
Mean coverage	115.54X	62.72X	50.52X	89.55X	178.37X	37.87X	64.66X	152.09X	71.76X	79.21X
Coverage at 10X	97.14%	95.23%	93.46%	97.08%	98.53%	89.33%	94.50%	98.42%	95.27%	96.29%

Individual	Subject 17	Mother 17	Father 17	Subject 18	Subject 19
Total reads	64,287,941	87,174,023	65,666,191	67,993,180	63,898,139
Mapped reads [a]	60,746,791 (94.49%)	74,376,740 (85.32%)	54,114,983 (82.41%)	61,170,223 (89.96%)	57,148,928 (89.4%)
Mean coverage	46.42X	51.34X	36.50X	50.71X	47.14X
Coverage at 10X	87.98%	87.29%	83.86%	88.37%	87.77%

[a] Inside of regions – capture region size = 2.27% of human genome

Table S4: Filtering data from exome sequenced families

Family	Subject 01	Subject 02	Subject 05	Subject 17	Subject 18	Subject 19
Total variants	204,358	201,364	201,362	42,070	?	?
Rare variants[a]	5,133	3,980	4,092	3,799	6,288	6,180
De novo variants	177	106	114	15	n/a[b]	n/a[b]
Protein altering variants	6	1	4	2	42	58
Sanger confirmed candidates	2[c]	1	3[d]	2[e]	1	1
Disease causing variant	*MAP3K7*: c.1454C>T, p.Pro485Leu	*MAP3K7*: c.1454C>T, p.Pro485Leu	*MAP3K7*: c.1454C>T, p.Pro485Leu	*TAB2*: c.1705G>A, p.Glu569Lys	*MAP3K7:* c.208G>C p.Gly70Gln	*MAP3K7:* c.299T>A p.Val100Glu
Depth of coverage at disease causing variant (reads/total reads)	16/29	10/37	18/31	15/39	24/74	3/7

[a] See methods for rare variant filtering protocol
[b] No parental sequence available
[c] MAP3K7 NM_003188, c.1454C>T; PIKFYVE NM_001178000, c.977C>T
[d] MAP3K7 NM_003188, c.1454C>T; MAPK8IP2 NM_012324, c.2068G>A; NOA1 NM_032313, c.88C>G
[e] EFHC1 NM_018100.3, c.674C>G; TAB2 NM_015093.5, c.1705G>A
N.B. Data in this table is presented from sequential filtering steps